CORROSION INVESTIGATION OF STRUCTURAL TRANSITION JOINTS THROUGH SCANNING ELECTROCHEMICAL MICROSCOPY AND THE CHARACTERIZATION OF HIGH-TEMPERATURE COATINGS AT DIFFERENT TEMPERATURES

A Thesis
Submitted to the Graduate Faculty
of the
North Dakota State University
of Agriculture and Applied Science

By

Luke Peter Wiering

In Partial Fulfillment of the Requirements
for the Degree of
MASTER OF SCIENCE

Major Department:
Coatings and Polymeric Materials

February 2021

Fargo, North Dakota

North Dakota State University
Graduate School

Title

CORROSION INVESTIGATION OF STRUCTURAL TRANSITION JOINTS THROUGH SCANNING ELECTROCHEMICAL MICROSCOPY AND THE CHARACTERIZATION OF HIGH-TEMPERATURE COATINGS AT DIFFERENT TEMPERATURES

By

Luke Peter Wiering

The Supervisory Committee certifies that this ***disquisition*** complies with North Dakota State University's regulations and meets the accepted standards for the degree of

MASTER OF SCIENCE

SUPERVISORY COMMITTEE:

Dr. Dante Battocchi
Chair

Dr. Dennis Tallman

Dr. Svetlana Kilina

Approved:

April 14, 2021
Date

Dr. Dean Webster
Department Chair

ABSTRACT

Scanning electrochemical microscopy is a method that incorporates an ultramicroelectrode capable of facilitating electrochemical reactions paired with an XYZ positioning system capable of micron-level movements. This study investigates the corrosion behavior of structural transition joint clad material that contains steel, pure aluminum, and an aluminum alloy blast welded into a single joint. This study will characterize the corrosion response of the structural transition joint and identify the galvanic activity measured between its layers.

High-temperature coatings in this study are designed to be used effectively up to 1400°F. In this study, we characterized several commercial high-temperature coatings exposed to different levels of heat. General trends of decreasing barrier performance were observed with the exception when these coatings are exposed to their rated temperature limit of 1400°F, at which the barrier increased slightly, indicated by their low-frequency impedance modulus. The cause is a combination of sintering and oxide formation.

ACKNOWLEDGMENTS

I would like to thank my advisor, Dr. Dante Battocchi for his help and guidance before and during my studies in the graduate school. I would like to thank Dr. Dennis Tallman for his preliminary work on SECM which accelerated me into the understanding and effective use of the device and for taking the time to be a part of my supervisory committee. I would like to thank Dr. Svetlana Kilina for your passion for the sciences, drive to teach your students, and for taking the time to be a part of my supervisory committee. I would also like to thank Dr. Xiaoning Qi and Dr. Vinod Upadhyay for their help, guidance, and wisdom during my time studying at NDSU. I would also like to thank the entire Department of Coatings and Polymeric Materials for the support in my research and the approachability and support of all staff.

I would like to thank Mr. Neil Witte and Mrs. Sharon Jensen, for sparking the love of science and challenging me to question, learn, and explore the world around me. Thank you both for your passion in what you do and know that it has meant a lot to me.

Lastly, I would also like to thank my wife, Ryley, for your endless support and patience during my studies. You bring me happiness and joy every day.

DEDICATION

This work is dedicated to Mark and Joan Wiering.

Your unending love, support, and appreciation have turned me into the man I am today.

Even though you rarely understood my work or studies,

you always understood its importance to me, and I am eternally grateful for that.

TABLE OF CONTENTS

LIST OF TABLES

LIST OF FIGURES

CHAPTER 1. INTRODUCTION TO CORROSION, GALVANIC CORROSION, AND CORROSION MITIGATION METHODS

1.1. Introduction to Corrosion

For thousands of years, humans have slowly been changing the landscapes and the materials of the earth for the advancement of society. The industrial revolution brought upon unprecedented growth, prosperity, and innovation that saw the need for crucial resources. The ability to effectively exploit the resources of the land forms the foundation of our modern society. Our mines dig and harvest the ore that has been stored since the formation of the earth to create infrastructure, transportation, buildings, and so much more. The most important resources that we mine out of the ground are metals. The metals exit the ground in the form of crude minerals. These consist of oxides, hydroxides, and complexes that are impure and unusable in their current form. We enact high-energy processes to isolate the metals into forms that we can use to create the alloys and materials with the needed strength and property characteristics to be used effectively. Unfortunately, this is not the end of the story. These metals, depending on environmental factors, begin degrading and oxidizing as they begin the process we know as corrosion.

Corrosion is defined as the spontaneous electrochemical reaction of metals returning to oxidized states caused by environmental conditions. This natural process occurs to some extent on the surface of most metals causing unwanted characteristics ranging from a tarnished surface finish to complete failure of structural integrity. The environment allows this process to initiate and propagate. Salt water, humidity, rain, and many other moisture-sources all cause corrosion on metal surfaces. These environmental factors are found all around the world and are realistically inescapable. Corrosion affects every part of society. Everything from infrastructure

to the metal in our cars are constantly under attack from corrosion. This widespread and constant degradation is a large cause of expense in the United States. It is estimated that in 2002, the estimated cost of corrosion in the U.S. for all sectors is $276 billion or 3.1% of GDP.[1] This cost is a burden on society and causes wasted downtime, production, and costs. Given the unprecedented growth of the U.S. GDP since 2002, this number can be extrapolated to much higher with estimates ranging to a possible $1 trillion of direct and indirect corrosion impact in the present day.[2] Large costs due to corrosion is cause enough for its prevention and management to be a priority, but unchecked corrosion also leads to loss of life and accidents through the degradation of buildings and infrastructure.

Now that the importance of corrosion control is established, the chemical side of corrosion will be explained. As stated above, corrosion is a spontaneous electrochemical reaction that happens at a metal's surface. There are four required aspects needed for corrosion to occur. These include an anode, cathode, electron transfer, and ion transfer. The anode and cathode form spontaneously. The electrical transfer is typically formed through the conductive metal to allow electrons to flow from the anode to the cathode. The ionic transfer is formed to allow the generated ions to neutralize in solution to complete the circuit. This is usually performed above the metal's surface through a solution media such as a water droplet, moisture deposition, the ocean. Figure 1.1 shows a diagram of common metal corrosion. Metal is oxidized at the anode. This allows free electrons to travel to the cathode to reduce dissolved oxygen present in the solution. The generated hydroxide ion, dissolved oxygen, and water all can form metal complexes from the generated metal cation. The product of these ions forming complexes is known as rust in iron corrosion. This process is simplified here and can include many different redox reactions of many different molecules.

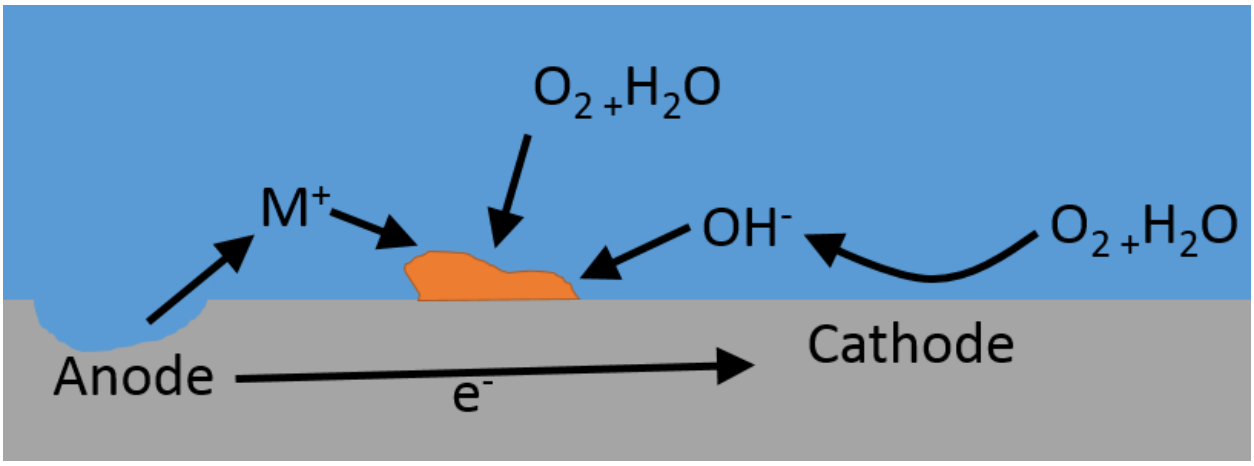

Figure 1.1. Corrosion cell on metal surface submerged in a corrosive solution. The letter "M" is a placeholder for any metal ion involved in the corrosion process.

The chemical reactions that Figure 1.1 portrays at the anode and cathode are displayed in Equations (1) and (2) respectively. Equation (3) is also a common reaction to occur at the cathode which generates hydrogen gas. These equations form the backbone of corrosion chemistry.

$$M = M^{+} + e^{-} \tag{1}$$

$$O_2 + 4e^{-} + 2H_2O = 4OH^{-} \tag{2}$$

$$2H^{+} + 2e^{-} = H_2 \tag{3}$$

1.2. Galvanic Corrosion

There are many types of corrosion that occur based off the types of metals and the orientation of metals and surrounding materials. One type of corrosion will be focused on primarily in this thesis. Galvanic corrosion is corrosive interaction of dissimilar metals. When two dissimilar metals share an electrical and ionic pathway, the more active metal will have predominantly anodic activity while the less active metal will have more cathodic activity. This process stems from the inherently different qualities that metals have with respect to their electrode potentials. We can measure the electrode potential by measuring the open circuit

potential (OCP) of metals in an electrochemical cell. The difference in OCP of different metals becomes the driving force for galvanic corrosion to occur. The ranges of electrode potentials are put into a table of most active (anodic) to most noble (cathodic). This table is called a galvanic series and is shown in Figure 1.2.

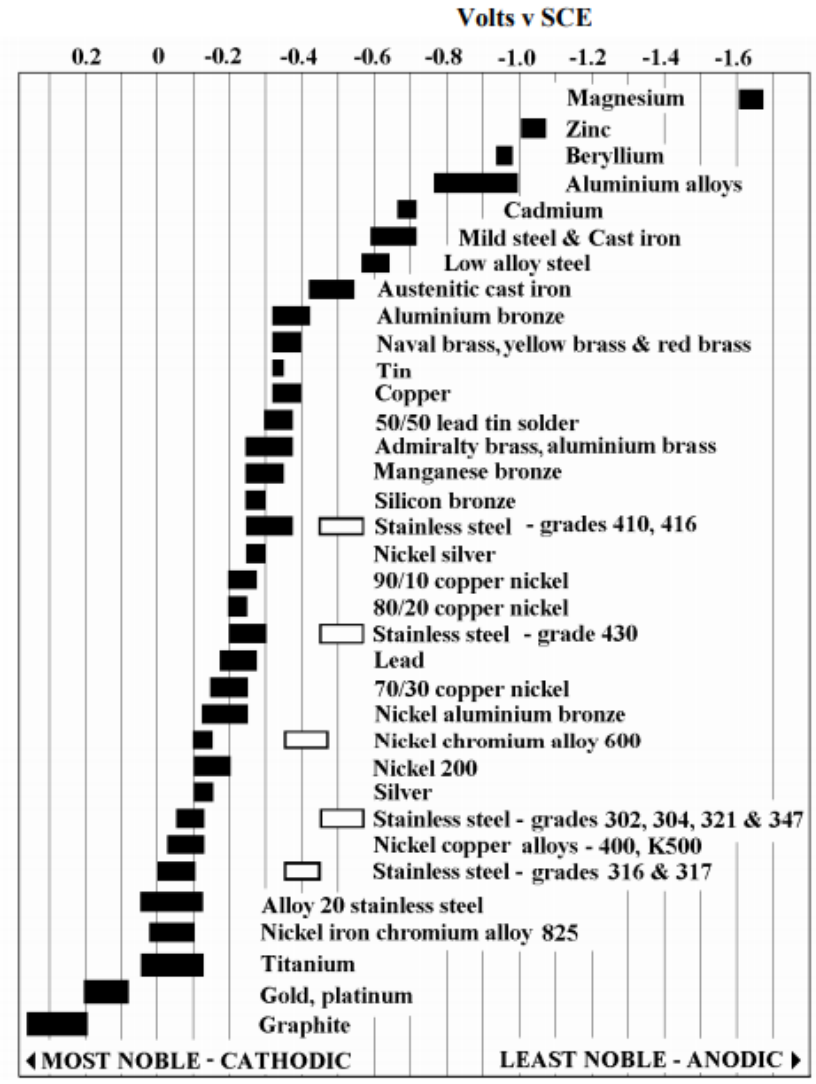

Figure 1.2. Galvanic series of metals in seawater. The most noble metals are on the bottom and the most active are at the top. The X-axis displays the OCP of metals with more cathodic lying to the left of the table and more anodic metals lying to the right. The more negative a metal's OCP is, the more anodic in character it is. The black bars represent the range of OCP corresponding to the metal listed to its right or left in the case of magnesium.[3]

The galvanic table in Figure 1.2 displays many commonly occurring metals and alloys. The difference range in potential between two metals typically corresponds to the extent of the galvanic corrosion interaction. Magnesium has a very negative OCP and thus would act strongly anodic when connected to any other metal on the table. Alternatively, graphite would act very with a strong cathodic response when connected to another metal. Aluminum has OCP ranges

from -0.75V vs SCE to -1.0V vs SCE. When Al is coupled with a mild steel, which has an OCP of -0.5V to -0.7V, the Al will take on anodic character while the steel will take on predominantly cathodic activity. That same Al can then be coupled with magnesium and become cathodic with the magnesium becoming anodic. These comparisons can be made throughout the table with metals acting anodic to metals with a less negative OCP, and metals .acting cathodic to metals with a more negative OCP. An example of galvanic corrosion is shown in Figure 1.3.

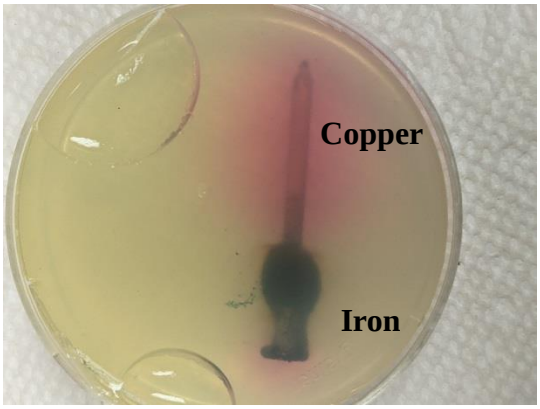

Figure 1.3. A galvanic corrosion interaction is displayed in agar gel. The iron nail has been half-plated with a film of copper using electrolysis. The agar contains an indicator which will turn pink in the presence of a base (cathodic) and an indicator that turns blue in the presence of iron ions (anodic).

The more noble copper displays cathodic activity due to the generation of hydroxide at the cathode causing the pH to drop and the indicator to display a pink hue. The more active iron near the head of the nail is anodic in nature and releasing oxidized iron ions which is being indicated by the dark blue indicator in the agar. This same process of galvanic corrosion can be used to prevent corrosion through a method named passive galvanic cathodic protection. This process starts with a metal structure that is chosen to be protected. This may be the hull of a ship or structural steel. The next step is to identify a more active metal, called the sacrificial anode, on the galvanic series to electrically connect periodically to the structure. An example of this would be zinc or magnesium due to their highly negative OCPs. The metals are joined together with

special care to make sure the sacrificial anode is exposed to the elements and not concealed or coated. As the system is exposed to the environment, the sacrificial anode will oxidize rapidly due to the accelerated anodic activity and would need to be replaced when thoroughly withered. The result would be the original structure being protected from corrosion while replacing the anode periodically. Examples of real life applications of this idea include anodes for maritime use, galvanized steel, and galvanized nails.

1.3. Introduction to the Use of Protective Coatings

Another very common way to prevent corrosion is through the use of coatings and paints. Coatings are defined in this thesis as a polymer-based film deposited onto a surface through a solvent medium and cures once deposited. The coating's purpose is to provide protection from the environment by acting as a physical barrier. Coatings provide an effective way to protect metal substrates from corrosion by limiting the ionic transfer through acting as a barrier to moisture. Many factors affect the success of coatings. Adhesion, thickness, water-uptake, and other factors all decide how well a coating may protect the substrate. Despite the advantages of coatings, there are downsides. Coatings offer limited permeability. This allows certain ions and molecules to penetrate the coated barrier to either degrade the coating's ability to act as a barrier, initiate corrosion underneath the coating, or both. This permeation can cause the adhesion of the coating to weaken and degrade which would increase in the susceptibility of the substrate to environmental conditions.[4] Coatings also fail due to physical impact and wear. Coatings are typically soft in nature due to their polymeric makeup when compared to most materials such as metals or ceramics.[5] Environmental factors like UV from the sun, heating/cooling, freezing/thawing, and acidic rain can all degrade coatings.[5] Coating design heavily depends on the desired application. Usually, desired characteristics of a coating come at the expense of other

characteristic's performance.[5] Despite the fallbacks of coatings, they still perform to great success, and development in the field of study allows better, cheaper, and more environmentally friendly.

1.4. References

(1) NACE International. *Corrosion Costs and Preventive Strategies in the United States*; 2002.

(2) NACE International. *International Measures of Prevention, Application, and Economics of Corrosion Technologies Study*; 2016.

(3) Atlas Steels. *Galvanic Corrosion, Atlas Tech Note No. 7*; 2010; Vol. Aug.

(4) McCafferty, E. *Introduction to Corrosion Science*; 2010. https://doi.org/10.1007/978-1-4419-0455-3.

(5) Oswald, T.; Menges, G. *Materials Science of Polymers for Engineers*; Hanser/Gardner: Germany, 1996.

CHAPTER 2. SCANNING ELECTROCHEMICAL MICROSCOPY: AN OVERVIEW OF COATING AND CORROSION APPLICATIONS

2.1. Abstract

Scanning electrochemical microscopy, or SECM, is a useful local electrochemical measurement technique that is being applied increasingly in corrosion and coatings research. The technique is capable of high resolution, local electrochemical potentiometric and amperometric measurements on active and passive surfaces. It uses the oxidation and reduction of a specific species in solution to investigate properties and events occurring near the surface of materials. The application of this device in corrosion and coating research grows constantly and provides more new and useful information. This review will explore in detail the background of SECM and its applications in corrosion and coatings research.

2.2. Introduction

Scanning electrochemical microscopy (SECM) is a method within scanning probe microscopy that utilizes an ultramicroelectrode (UME) to study, regulate, and measure local electrochemical reactions. SECM as a method was introduced by Bard et al in 1989, but similar scanning probe techniques were first demonstrated by Engstrom in 1987.[1,2] It incorporates local electrochemical monitoring with fine and coarse XYZ positioning. A solution is used as the medium where SECM measurements are taken. A particular chemical species within the solution is typically targeted for reduction or oxidation by the UME at the tip. The selectivity of this species is controlled through the UME acting as a WE while maintaining a selected potential through the use of a potentiostat. The responding tip current created from the redox reaction is then measured.

SECM has the potential to monitor many of the electrochemical reactions that take place in corrosion. The reactants and products of these reactions can be monitored by SECM using one of the modes of operation. SECM can be utilized to identify the different stages of corrosion.

2.2.1. Schematic of Electrochemical Cell Configuration

The SECM is typically configured in a 3-electrode layout as shown in Figure 2.1. The sample is submerged in solution with adequate conductivity to conduct experiments. The reference and counter electrodes are present in the solution. The working electrode is present as the UME in the cell. The UME is capable of XYZ-axis movement with high resolution through the use of piezo motors. A second working electrode is present to optionally polarize the sample. The UME is typically locked at a known height above the sample while scanning along the XY-axes. There are select applications of the SECM in corrosion and coating research that lock the XY-axes while manipulating the Z-axis such as artificial pit propagation and film-penetrating studies.[3]

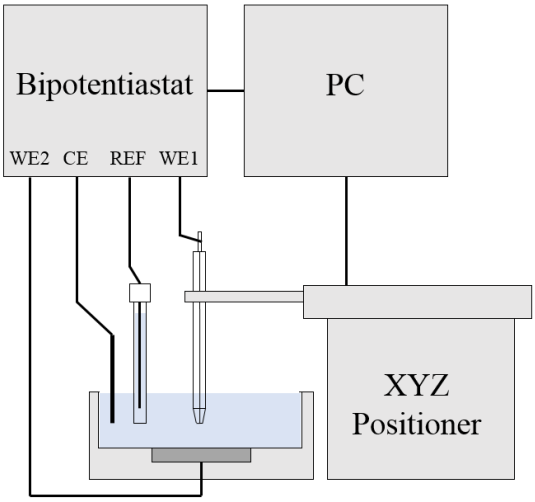

Figure 2.1. Layout of SECM. The PC is used as the interface to control, view, and process data from the SECM through the connections to the positioning system and bipotentiostat.

2.2.2. Theory of SECM Operation

The basis of SECM measurements depend on the phenomenon of feedback mode. As shown in Figure 2.2, the current response of an electrochemical reaction facilitated by the UME is dependent on the surface of the material being studied and how it affects the hemispherical diffusion of mediator to the exposed electrode disk. When the UME tip has a diameter much larger than the disk electrode diameter, the current response is dependent on Equation 4.

$$i_{\infty} = 4nFDCa \tag{4}$$

In (4), i_{∞} is the current response, n is the number of electrons, D is the diffusion coefficient, C is the mediator concentration, and a is the radius of the UME.[1]

A use of SECM becomes apparent when the current is affected by the surface or interface of a substrate as shown in Figure 2.2. If the substrate is conductive and capable of reversing the redox reaction at the tip, a positive feedback response is to be expected at the tip resulting in increased current as the tip approaches the conductive substrate as shown in Figure 2.2B. If the tip approaches an insulating substrate, the hemisphere of diffusion becomes constricted. This limits the diffusion of mediator to the tip to undergo a reaction. This reduction in diffusion to the electrode results in a decrease in current [as per (4)]. This phenomenon is known as negative feedback. More frequently used SECM measurements are via the positive and negative feedback modes. Other modes of operation are possible as well. These include substrate generated/tip collected, substrate collected/tip generated, alternating current (LEIS), and redox competition.

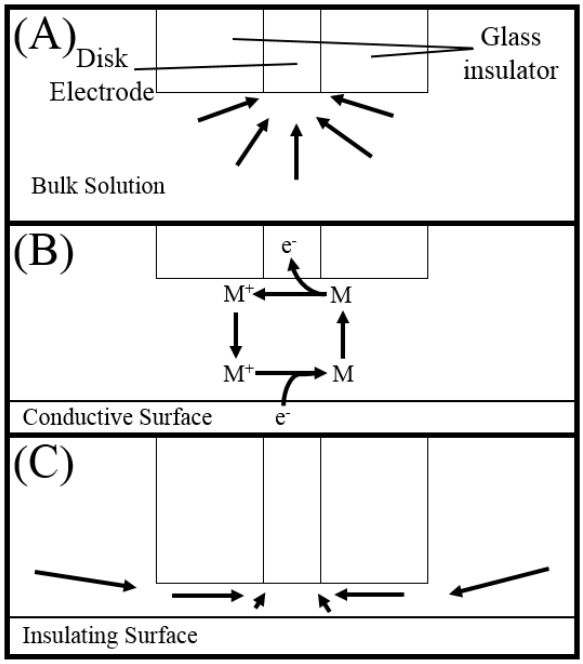

Figure 2.2. Modes of diffusion in SECM mediation: (A) Bulk Solution, diffusion-controlled; (B) Positive Feedback; (C) Negative Feedback. Both (B) and (C) can occur at similar probe heights from the substrate.

Substrate generated/tip collected, SG/TC, is a mode of operation where the substrate, coating, or interfacial system release a target chemical species. The tip is then scanned through these local concentrations near the surface of the substrate. Increases in current are usually observed as increases of these substrate-originated species. Common applications include substrate-originating mediators, smart coatings, inhibitors, and corrosion product sensing. This can be applied by detecting certain products of corrosion with the tip originating from the processes occurring at the substrate surface.

Substrate collected/tip generated, SC/TG, is the opposite of the above-mentioned method. The tip generates a particular species that either reacts with the coating/substrate/system or undergoes a redox reaction at the substrate and observed at the substrate through the second working electrode with the bipotentiostat. This method has application in micro-etching and artificial pit generation. By generating specific substrate-reactive species with the tip, precise,

local concentrations can be selectively placed on a substrate to initiate a reaction local to the tip location.

Alternating current SECM (AC-SECM) employs very similar theory as electrochemical impedance spectroscopy to study interfaces and coating characteristics. LEIS is also possible in this mode to map out areas of possible local EIS differences. Advantages of AC-SECM are similar to common global EIS; the small alternating potential of the tip does not influence the electrochemical makeup of the solution or substrate. This allows measurements to proceed and be measured in a more controlled fashion without disturbing present species.

Yet another significant measurement mode is also known as redox competition mode. This involves a redox-active species present in solution that undergoes a nonreversible reaction at both the substrate and tip. This creates a "competition" between the two point of consumption. Tip scanning records constant current throughout a solution or substrate surface except where current drops where the substrate is consuming that species thus starving the tip. A common application is O_2 reduction which will be explained further in this review.

2.3. Modes of Operation in Corrosion and Coating Applications

2.3.1. Identifying Corrosion Before Initiation

Many methods/techniques can detect active and past corrosion. A true challenge would be to predict corrosion through precursor activity at the substrate surface. SECM has the capability to measure changes in mediators that are influenced and created by precursor sites to corrosion. The pitting of Ti can be predicted using SECM with a Br^- indicator as performed by Casillas and colleagues.[4] Halide ions have been shown to cause disruption of the Ti/TiO_2 protective layer. SECM was applied to map out areas of high Br^- oxidation into Br_2. The study showed the correlation of increased electron-transfer rates for Br^- oxidation with the locations of

future artificial pits. Increased electron activity within the oxide film may be the pre-cursor for pitting on Ti surfaces. This activity also appears to be linked to the Br^- oxidation measured by the SECM tip.

A precursor to pit propagation is the formation of metastable pits on the surface of stainless steel. This was observed by Gonzalez-Garcia et al.[5] SECM was employed to oxidize Fe^{+2} ions diffusing from the metastable pit locations. High positive potentials ranging from 0.547 to 1.077 V(SHE) were used to polarize the UME. The scanning height was 10μm above the stainless steel sample. The locations of Fe^{+2} oxidation were short lived, intermittent, and unrepeatable within the same scan. The inconsistency of these readings was concluded to be indicative of the observation of metastable pits rather than propagating pits with lifetimes of the metastable pits predicted to be <6 seconds. Zhu and Williams have performed similar work on stainless steel on a much smaller scale of 60x60μm and 0.5μm probe height with results that were less conclusive.[6]

2.3.2. Corrosion Initiation

The initiation of corrosion has always been an area of interest to investigate what environment and components accelerate or restricts the process of corrosion. SECM has the capability to initiate localized corrosion through creation of a local, corrosive species generated by the tip. Pit formation is possible through the precision that the SECM tip provides. An example would be the production of chloride ions to facilitate the breakdown of an iron passive layer. Trichloroacetic acid was used as the source of chloride ions. A bipotentiostat was utilized to control both a gold UME and an iron electrode. A passive layer was formed on the iron electrode by applying a passivating potential for 0.5 seconds. Chloride ion creation was then initiated. Pit initiation and propagation then occurred. The results were then observed via optical

microscope to confirm the presence of the pit. Current was being measured throughout the entire process of both the tip and the iron electrode. The results of the study showed that grain boundaries of the iron electrode had a large impact on the successfulness of pit initiation. Grain boundaries are typically locations of higher pit activity. This was observed when the UME was in between grain boundaries and pit formation was less likely. Pits were successfully formed on iron substrates.[7]

A similar study with SECM assisted electrochemical quartz crystal microbalance, EQCM, was conducted. EQCM is a device that can measure nano-scale changes in mass. The combination of SECM and EQCM allowed "simultaneous measurements of potential, current, and mass variations to be performed."[8] Iron atoms were deposited onto the EQCM and analyzed with the UME of the SECM. Chloride ions were generated at the tip through the reduction of silver chloride in solution to initiate and propagate pitting. The pH was also variable to record the pit propagation response. It was observed that pit propagated faster and with less chloride at lower pH and slower at higher pH.[8]

2.3.3. Metal Corrosion Studies

The study of the corrosion cell is possible with SECM. The cathode of a corrosion cell can involve the reduction of dissolved diatomic oxygen. This reduction of oxygen to hydroxide creates a localized, oxygen-depleted location near the surface of the metal that is displaying this cathodic activity. SECM can reduce oxygen through the reduction into hydroxide to create a redox competition mode that allows the UME tip to compete with the cathodic metal substrate for oxygen to undergo reduction.[9–12] Identification of cathodic areas can be extrapolated to locate areas of predominate anodic activity. This method is useful in galvanic corrosion studies. The galvanic interaction between aluminum and magnesium has been studied to test the possibility of

magnesium as a sacrificial anode/substrate. Aluminum was connected to magnesium via an electrical switch in a single cell. SECM scans showed an increase in cathodic activity of the aluminum when connected to magnesium than not, as shown in (1) of Figure 2.3. Also shown, is the amperometric scan of magnesium isolated and connected to the aluminum electrode in (2) of Figure 2.3. A local drop in oxygen concentration observed in both (2a) and (2b) of Figure 2.3 shows that oxygen reduction still occurs at the surface of magnesium even while electrically connected to a more noble aluminum.[9,10]

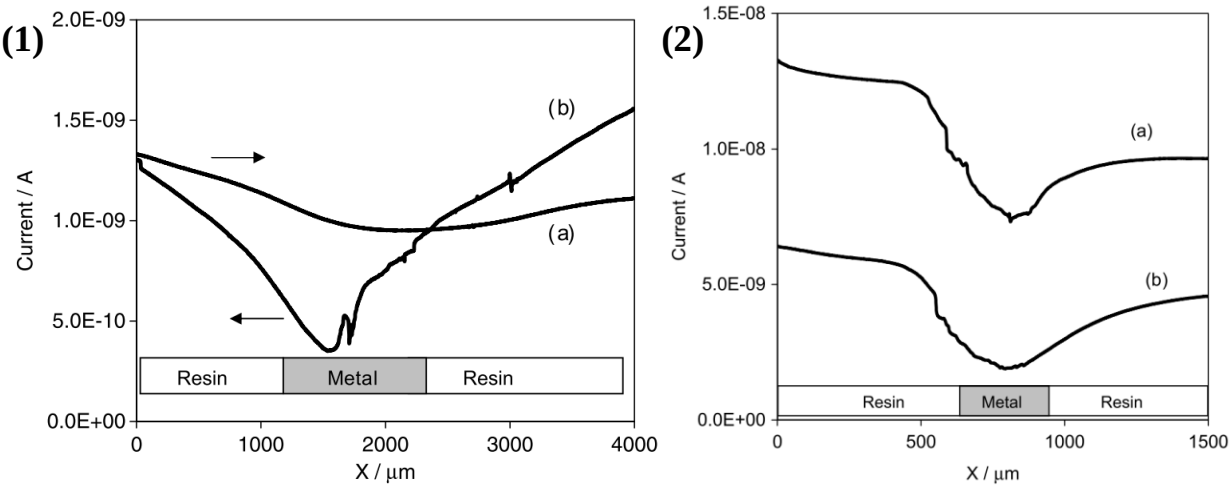

Figure 2.3. Amperometric scans obtained at -0.75V vs Ag/AgCl. (1) shows AA2024 aluminum scanned at a height of 500µm while (1a) isolated and (1b) cathodically protected by magnesium anode. (2) shows magnesium scanned at 200µm above the electrode. (2a) an isolated electrode and (2b) connected to aluminum electrode.[10]

Several investigation have been performed on metal substrate-solution interactions utilizing SECM. AZ31 magnesium was analyzed submerged in simulated biological fluid with SECM. The goal of the study was to analyze the possibility of utilizing magnesium in biological systems. This was approached by identifying areas of high activity on the magnesium sample's surface when exposed to the simulated biological fluid. Feedback mode with ferrocene methanol was used to identify areas of electrochemical activity. H_2 was observed under SG/TC at 0.0V vs Ag/AgCl to monitor sites of hydrogen gas generation. AC-SECM was used to analyze the

magnesium sample as well. An excitation signal of 100mV in amplitude at 1 kHz was used to identify areas of conductivity on the surface layer of the magnesium. The final use of SECM was potentiometric mode to map local pH values on the magnesium. An Ir/IrOx UME was used to measure local pH. The open circuit potential of the Ir/IrOx UME was measured at different pH to create a calibration curve to correlate observed OCP to pH. The locations of high pH correlated well with areas of H_2 generation and low surface resistivity.[13]

AC-SECM has also been used to study AA2024 aluminum. Area scans of a sample of aluminum were conducted at different frequencies over increasing immersion time. The UME had an AC signal with an amplitude of $10mV_{pp}$ at two different frequencies, 55kHz and 7kHz. This method allowed localized modulus and phase angle to be mapped on the surface of the aluminum to identify areas of passive layer weakening.[14]

Stainless steel pit initiation and propagation can be tracked through Fe^{+2} oxidation while using the SECM in SG/TC mode. A sample of stainless steel was analyzed with SECM with a solution of 0.1M NaCl and 10mM KI. Anodic current was applied to the steel to facilitate pit formation. These pits were then identified and scanned at a tip potential of 0.56V vs SCE. This anodic tip potential allowed Fe^{+2} to be oxidized into Fe^{+3}. The presence of I^- in solution allowed greater peaks to be measured when observing Fe^{+2} in solution. The generated Fe^{+2} was measured through SG/TC but also interacted with the I^-/I_3^- feedback loop observed at the tip. This combination allowed sharper and taller spikes in current to be measured with SECM. Findings of this work included increased Fe^{+2} activity in increasingly anodic conditions. Also, stages of pit initiation were observed by polarizing the stainless steel through increasing anodic potentials while scanning. The observation of a feedback phenomenon while performing SG/TC techniques could provide insight into stainless steel corrosion mechanism.[15]

2.3.4. Coatings Application

The coatings industry is very important in the application of corrosion prevention. The use of coatings spans the entire globe and is a multi-billion-dollar industry. Many global methods of coating performance are used widely with great success and dependability such as EIS. SECM has the capability of analyzing coating performance at a local level. This section explores SECM methods to analyze the performance of coatings and to characterize the failure of a coating. This is performed either through an artificial defect or through accelerated weathering of a coated system.

SECM can be applied to undamaged coatings to analyze coating properties. AC-SECM while approaching inhibitor-containing coatings could possibly be used to monitor inhibitor properties. AC-SECM has been used to accurately determine the probe-approach curve in SECM. This curve was observed to change as an inhibitor-treated copper sample was approached at different frequencies of AC signal. A change in positive and negative feedback characteristics of the curve could show the gradual reduction of electron transfer by the organic inhibitors. This phenomenon was measured over different time lengths and with different inhibitors present. Advancements in this method could lead to new options to characterize corrosion inhibitors.[11]

Feedback mode has the ability to monitor surface topography. A sample of coil coated polyester on steel was used in the study. Ferrocene-methanol was used as the mediator to monitor topography. Dissolved oxygen reduction was also used in feedback mode to compare any possible unintended coating/ferrocene-methanol interaction. The ferrocene mediator was used in three different solutions: 0.1M KCl, 0.1M K_2SO_4, and 0.1M KNO_3. The variety of salt solutions used were to analyze any particular effects that an anionic presence might have on the coating. The sample was scanned in feedback mode 10μm above the surface in an area

200x200µm. The sample was scanned periodically over 24 hours to show any possible change in the coating surface. General swelling was observed over time by all electrolyte solutions. Roughening of the surface was observed by SECM in the 0.1M KCl solution. This was attributed to the chloride ions having an effect on the coating. A local swelling was observed as well in the same sample. The experiment was replicated with dissolved oxygen reduction and similar results were observed. The authors concluded that these observations were from the early stages of blistering. This method could be used in further applications of accelerated characterization of coating systems.[16–19] The study was continued by the authors to confirm that SECM is fully capable to recognize blister nucleation but would need longer times to observe coating failure at these sites.[20] Room temperature ionic liquid has been used as the conductive liquid in SECM experiments. A study was conducted that intended to use the topographical data-collection of SECM on a coating that swells when temperature is increased. RTIL was used to mitigate any solution-based swelling that water would cause. The SECM successfully recorded negative feedback in an RTIL with 1mM $K_4[Fe(CN)]_6$ used as the mediator. The findings concluded that the swelling was observed via SECM with the absence of a water-based solution.[21]

The ultramicroelectrode tip has the ability to be inserted into a coating to monitor potential, kinetic, and thickness of the coating.[3] This study was unique when compared to other research conducted with SECM since its advent. The purpose of this study was to observe the feedback mode through a solid film. Instead of solution carrying the mediator, a conductive coating of Nafion was used to contain the mediator, $Os(bpy)_3^{2+}$. The mediating reaction is shown in (5). The forward reaction of (5) could be achieved through a tip potential of +0.80V vs SCE.

$$Os(bpy)_3^{+2} \leftrightarrow Os(bpy)_3^{+3} + e^- \quad (5)$$

The substrate was an indium tin oxide surface. The substrate had a potential of +0.20V vs SCE to cause the reverse reaction of (5) to take place at the substrate. This combination of potentials allowed a positive feedback loop to take place as explained in Figures 2.4 and 2.5. The results of the test were that a definitive current response The significance of this study is the possibility of utilizing SECM to analyze and characterize coatings throughout the coating thickness.[3]

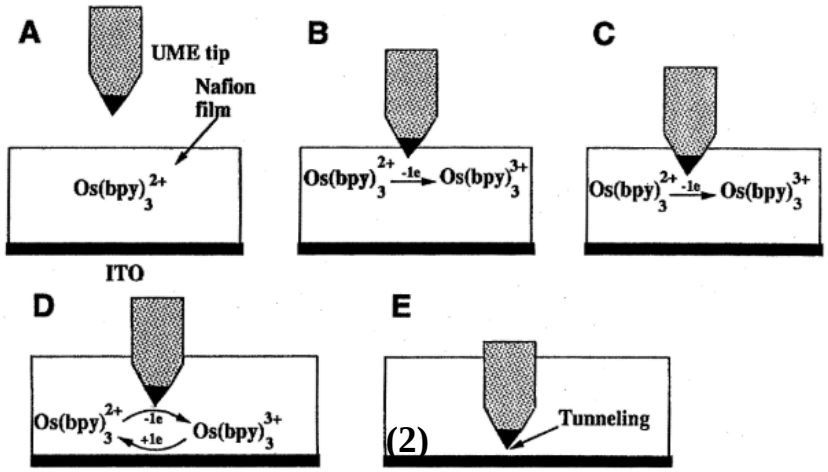

Figure 2.4. Depicted are the events that occur at the tip when it was inserted into the Nafion coating. **A:** The UME approaching the surface of the coating. **B:** The conical tip penetrates the coating and begins oxidizing the $Os(bpy)_3^{+2}$ mediator. **C:** The tip has now fully penetrated the coating and has achieved a steady-state, diffusion-controlled current. It is too far from the ITO substrate to receive any positive feedback. **D:** The tip has now approached close enough to the substrate to begin a positive feedback mode with the substrate. **E:** The tip is close enough to the substrate that tunneling effects between the tip and the substrate begin to increase current.[3]

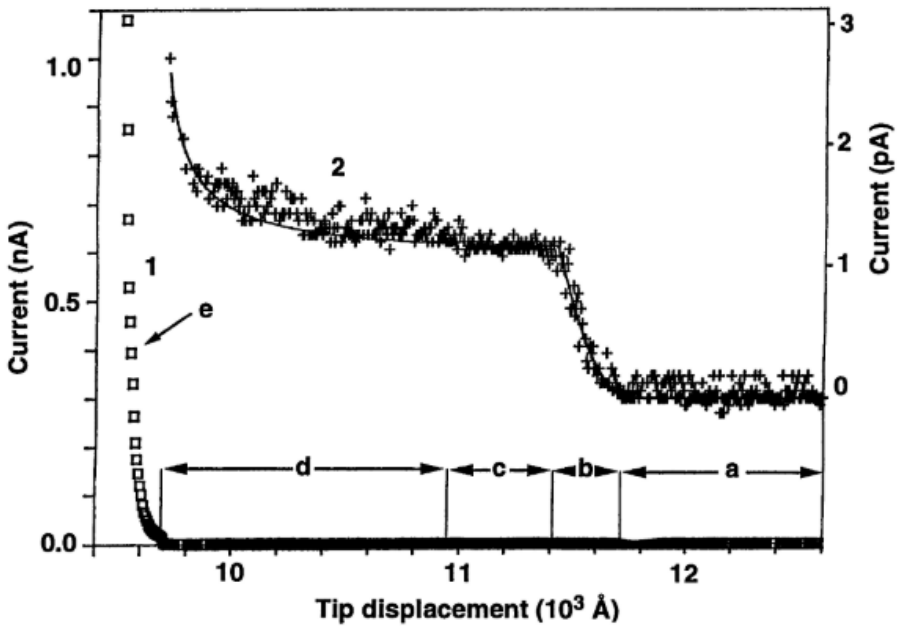

Figure 2.5. Curves 1 and 2 display the current response of the cone-tipped UME as it penetrates the Nafion coating. Curve 2(right) displays the current response of the tip as it proceeds through steps **A**-**E** from Figure 2.4. Curve 1(left) displays the tunneling current on a scale that would be too large to view Curve 2. The tip was held at a +0.80V vs SCE and the substrate was held at +0.20V vs SCE.[3]

The anodic half-reaction of corrosion yields iron ions due to the oxidation of steel. This solubilized iron can be found as iron(II). Souto et al employed the SECM technique of substrate generated/tip collected to detect the presence of iron(II) at a holiday in an organic coating. Cyclic voltammetry showed that iron(II) can be further oxidized into iron(III) using the UME at potentials above 0.15V vs Ag/AgCl. The potential of 0.60V was used in the experiment. The results showed that a peak of current was observed directly over the holiday. This was concluded to be the presence of iron(II) ions being oxidized at the UME tip. No potential or applied current was impressed upon the substrate. This demonstrated method is able to directly measure and detect corrosion products of steel.[22]

AC-SECM can be employed to monitor the local integrity the coating on a lacquer tinplate. This study showed that similar modes of SECM operation can be performed in AC mode. Positive and negative feedback modes were performed with an AC amplitude of 10mV at 10kHz. Artificial scribes and holidays were created in the lacquer coating to test the AC-SECM response of conductive and nonconductive.[23]

Holidays and scribes are intentional defects that are carved into coatings on a substrate. These defects allow the analysis of the coating-defect. In the application of holiday analysis, feedback mode can be used over an intact coating using oxygen reduction. Once the UME scans over the holiday, the mode is switched to redox competition from negative feedback mode due to the presence of a corroding exposed substrate.[24,25] Xia et al conducted similar holiday research and was able to identify an initial increased rate of corrosion followed by the slowing of corrosion due to the buildup of corrosion products.[26]

This same feedback/redox competition method can be observed in self-healing coatings as well. Self-healing coatings contain microcapsules of polymer or catalyst that, when ruptured, release their contents with the intended design to flow and cure within the defect of the coating. SECM has been used to monitor and track the "healing" of these types of films. Using oxygen-reduction, one can track the corrosion process through the locating of cathodic areas. Linear scans over a scribe in a self-healing coatings containing silyl ester microcapsules were studied by Garcia et al.[27,28] The study describes the use of oxygen reduction to measure the corrosion process as a self-healing coating closed. Ferrocene negative-feedback mediation was used as well to monitor and topological changes within the scribe during the healing process. Within 15 days of the scribe being exposed, SECM showed that the competition mode of oxygen reduction started presenting more negative-feedback characteristics. This was concluded to be a

confirmation that the scribe "healed" due to the silyl ester film-formation. A similar investigation utilizing SECM involved linseed oil microcapsules to heal a scribe in an epoxy resin.[29] The study used the oxygen reduction competition mode as well as the SG-TC mode of the oxidation of Fe^{+2} ions using a +0.5V vs Ag/AgCl(sat'd) tip potential. This study also showed similar results of the oxygen and ferrous ion signatures disappearing from SECM scans as the scribe was filled with a protective film originating from the microcapsules.

Corrosion inhibition is the practice of adding a substance to a film to prevent corrosion from occurring at the substrate. Common practices include mixing these additives into the paint formulation or applying a pretreatment to a substrate prior to coating with a paint. SECM can use oxygen reduction to monitor corrosion activity within corrosion inhibited coatings on defects. The combination of oxygen reduction redox competition mode and ferrocene feedback mode allowed the study of a scribe in aluminum flake epoxy.[30,31] The study also included the addition of either tungstate- or vanadate-doped polypyrrole for corrosion inhibition. A scribe in this coating was monitored over time using SECM with the two above mentioned methods. By monitoring oxygen levels, they were able to track the presence of corrosion while also measuring any physical buildup within the scribe with the use of ferrocene with feedback mode.

SECM was used to show the corrosion mitigation caused by modified graphene oxide film deposited on galvanized steel surface. The mediator used to study the film was $K_4[Fe(CN)_6]$ with a UME potential of +0.5V vs Ag/AgCl. Feedback mode was instituted to measure the conductivity of the modified surface. Potassium ferricyanide is capable of a positive feedback when the UME approaches a conductive surface. The results of the experiment show that by increasing the concentration of the modified graphene oxide, the surface became increasingly nonconductive. Recorded currents over the highest concentration of additive showed current

lower than the bulk current indicating a negative feedback. Through the use of SECM, the researchers were able to show anti-corrosion behavior caused by a film on a metal substrate.[32] A similar study was performed by Fernández et al with the replacement of a magnesium substrate with modified graphene oxide deposited as a film. The results of the SECM experiment showed the film increasing corrosion resistance due to limiting of positive feedback caused by conductive surfaces by potassium ferricyanide.[33]

2.4. Future Progress of SECM and Calls for Study

SECM still has untapped potential as a method and device in corrosion science. Further understanding micro-concentrations of corrosion products and reactants of the anode and cathode could be achieved using the electrochemical sensitivity of SECM. Similarly, new mediators should be explored with relation to corrosion, currently there are only a few mediators used in studies. Substrate collected/tip generated (SC/TG) modes are under researched and have great potential due to the local generation of species that are either unstable or difficult to transport or study. Pit generation has been studied but has larger potential to expand upon because of its ability to monitor and analyze metastable pitting locations and pitting initialization.

2.5. Summary

Local electrochemical techniques are increasingly advancing the study of interfacial and solution related chemical phenomenon. SECM has the capability to monitor corrosion processes through the monitoring of the reactants and resulting products of corrosion. The scale of SECM allows the analysis of micro-scale corrosion events such as pitting as well as macro-scale scans such as galvanic coupling. Many modes are available to study corrosion. The usefulness and flexibility of these modes show that SECM can still being researched and has great promise to be expanded as a promising and impactful technique.

2.6. References

(1) Bard, A. J.; Fan, F. F.; Kwak, J.; Lev, O. Scanning Electrochemical Microscopy. Introduction and Principles. *Anal. Chem.* **1989**, *61* (2), 132–138.

(2) *Scanning Electrochemical Microscopy*; Bard, A. J., Mirkin, M. V, Eds.; CRC Press, 2001. https://doi.org/10.1201/9780203910771.

(3) Mirkin, M. V; Fan, F. F.; Bard, A. J. Measurements Inside a Direct Electrochemical 2000 Angstrom Thick Polymer Film by Scanning Electrochemical Microscopy. *Science (80-.).* **1992**, *257* (5068), 364–366.

(4) Casillas, N. Scanning Electrochemical Microscopy of Precursor Sites for Pitting Corrosion on Titanium. *J. Electrochem. Soc.* **1993**, *140* (9), L142. https://doi.org/10.1149/1.2220897.

(5) González-García, Y.; Burstein, G. T.; González, S.; Souto, R. M. Imaging Metastable Pits on Austenitic Stainless Steel in Situ at the Open-Circuit Corrosion Potential. *Electrochem. commun.* **2004**, *6*, 637–642.

(6) Zhu, Y. Scanning Electrochemical Microscopic Observation of a Precursor State to Pitting Corrosion of Stainless Steel. *J. Electrochem. Soc.* **1997**, *144* (3), L43. https://doi.org/10.1149/1.1837487.

(7) Still, J. W.; Wipf, D. O. Breakdown of the Iron Passive Layer by Use of the Scanning Electrochemical Microscope. *J. Electrochem. Soc.* **1997**, *144* (8), 2657–2665.

(8) Gabrielli, C.; Joiret, S.; Keddam, M.; Perrot, H.; Portail, N.; Rousseau, P.; Vivier, V. A SECM Assisted EQCM Study of Iron Pitting. *Electrochim. Acta* **2007**, *52*, 7706–7714.

(9) Simões, A. M.; Battocchi, D.; Tallman, D.; Bierwagen, G. Assessment of the Corrosion Protection of Aluminium Substrates by a Mg-Rich Primer: EIS, SVET and SECM Study. *Prog. Org. Coatings* **2008**, *63*, 260–266.

(10) Simões, A. M.; Battocchi, D.; Tallman, D. E.; Bierwagen, G. P. SVET and SECM Imaging of Cathodic Protection of Aluminium by a Mg-Rich Coating. *Corros. Sci.* **2007**, *49*, 3838–3849.

(11) Souto, R. M.; Socas, B.; Izquierdo, J.; Santana, J. J.; González, S. New Opportunities for the Study of Organic Films Applied on Metals for Corrosion Protection by Means of Alternating Current Scanning Electrochemical Microscopy. *Prog. Org. Coatings* **2012**, *74* (2), 371–375.

(12) Niu, L.; Yin, Y.; Guo, W.; Lu, M.; Qin, R.; Chen, S. Application of Scanning Electrochemical Microscope in the Study of Corrosion of Metals. *J. Mater. Sci.* **2009**, *44*, 4511–4521.

(13) Jamali, S. S.; Moulton, S. E.; Tallman, D. E.; Forsyth, M.; Weber, J.; Wallace, G. G. Applications of Scanning Electrochemical Microscopy (SECM) for Local Characterization of AZ31 Surface during Corrosion in a Buffered Media. *Corros. Sci.* **2014**, *86*, 93–100.

(14) Izquierdo, J.; González, S.; Souto, R. M. Application of AC-SECM in Corrosion Science: Local Visualization of Heterogeneous Chemical Activity in AA2024 Surfaces. *Int. J. Electrochem. Sci.* **2012**, *7*, 11377–11388.

(15) Yin, Y.; Niu, L.; Lu, M.; Guo, W.; Chen, S. In Situ Characterization of Localized Corrosion of Stainless Steel by Scanning Electrochemical Microscope. *Appl. Surf. Sci.* **2009**, *255*, 9193–9199.

(16) Souto, R. M.; González-García, Y.; Izquierdo, J.; González, S. Examination of Organic Coatings on Metallic Substrates by Scanning Electrochemical Microscopy in Feedback Mode: Revealing the Early Stages of Coating Breakdown in Corrosive Environments. *Corros. Sci.* **2010**, *52*, 748–753.

(17) Souto, R. M.; González-García, Y.; González, S. Characterization of Coating Systems by Scanning Electrochemical Microscopy: Surface Topology and Blistering. *Prog. Org. Coatings* **2009**, *65* (4), 435–439. https://doi.org/10.1016/j.porgcoat.2009.03.008.

(18) Souto, R. M.; González-García, Y.; González, S.; Burstein, G. T. Damage to Paint Coatings Caused by Electrolyte Immersion as Observed in Situ by Scanning Electrochemical Microscopy. *Corros. Sci.* **2004**, *46*, 2621–2628.

(19) Souto, R. M.; González-García, Y.; González, S.; Burstein, G. T. Imaging the Origins of Coating Degradation and Blistering Caused by Electrolyte Immersion Assisted by SECM. *Electroanalysis* **2009**, *21* (23), 2569–2574. https://doi.org/10.1002/elan.200900262.

(20) Souto, R. M.; González-García, Y.; González, S. Evaluation of the Corrosion Performance of Coil-Coated Steel Sheet as Studied by Scanning Electrochemical Microscopy. *Corros. Sci.* **2008**, *50*, 1637–1643. https://doi.org/10.1016/j.corsci.2008.02.019.

(21) Trinh, D.; Vosgien-Lacombre, C.; Bouvet, G.; Mallarino, S.; Touzain, S. Use of Ionic Liquids in SECM Experiments to Distinguish Effects of Temperature and Water in Organic Coating Swelling. *Prog. Org. Coatings* **2020**, *139* (September 2019), 105438. https://doi.org/10.1016/j.porgcoat.2019.105438.

(22) Souto, R. M.; González-García, Y.; González, S. In Situ Monitoring of Electroactive Species by Using the Scanning Electrochemical Microscope. Application to the Investigation of Degradation Processes at Defective Coated Metals. *Corros. Sci.* **2005**, *47* (12), 3312–3323.

(23) Katemann, B. B.; Inchauspe, C. G.; Castro, P. A.; Schulte, A.; Calvo, E. J.; Schuhmann, W. Precursor Sites for Localised Corrosion on Lacquered Tinplates Visualised by Means of Alternating Current Scanning Electrochemical Microscopy. *Electrochim. Acta* **2003**, *48*, 1115–1121. https://doi.org/10.1016/S0013-4686(02)00822-8.

(24) Souto, R. M.; Fernández-Mérida, L.; González, S. SECM Imaging of Interfacial Processes in Defective Organic Coatings Applied on Metallic Substrates Using Oxygen as Redox Mediator. *Electroanalysis* **2009**, *21* (24), 2640–2646.

(25) Santana, J. J.; González-Guzmán, J.; Fernández-Mérida, L.; González, S.; Souto, R. M. Visualization of Local Degradation Processes in Coated Metals by Means of Scanning Electrochemical Microscopy in the Redox Competition Mode. *Electrochim. Acta* **2010**, *55*, 4488–4494. https://doi.org/10.1016/j.electacta.2010.02.091.

(26) Xia, D.; Wang, J.; Wu, Z.; Qin, Z.; Xu, L.; Hu, W.; Behnamian, Y.; Luo, J. Sensing Corrosion within an Artificial Defect in Organic Coating Using SECM. *Sensors Actuators, B Chem.* **2019**, *280* (October 2018), 235–242. https://doi.org/S0925400518318148.

(27) González-García, Y.; García, S. J.; Hughes, A. E.; Mol, J. M. C. A Combined Redox-Competition and Negative-Feedback SECM Study of Self-Healing Anticorrosive Coatings. *Electrochem. commun.* **2011**, *13*, 1094–1097.

(28) González-García, Y.; Mol, J. M. C.; Muselle, T.; Graeve, I. De; Assche, G. Van; Scheltjens, G.; Mele, B. V; Terryn, H. SECM Study of Defect Repair in Self-Healing Polymer Coatings on Metals. *Electrochem. commun.* **2011**, *13*, 169–173.

(29) Pilbáth, A.; Szabó, T.; Telegdi, J.; Nyikos, L. SECM Study of Steel Corrosion under Scratched Microencapsulated Epoxy Resin. *Prog. Org. Coatings* **2012**, *75*, 480–485.

(30) Jensen, M. B.; Peterson, M. J.; Jadhav, N.; Gelling, V. J. SECM Investigation of Corrosion Inhibition by Tungstate- and Vanadate-Doped Polypyrrole/Aluminum Flake Composite Coatings on AA2024-T3. *Prog. Org. Coatings* **2014**, *77*, 2116–2122.

(31) Jadhav, N.; Jensen, M. B.; Gelling, V. Tungstate and Vanadate-Doped Polypyrrole/Aluminum Flake Composite Coatings for the Corrosion Protection of Aluminum 2024-T3. *J. Coatings Technol. Res.* **2015**, *12* (2), 259–276.

(32) Liu, Q.; Zhang, X.; Zhou, W.; Ma, R.; Du, A.; Fan, Y.; Zhao, X.; Cao, X. Improved Anti-Corrosion Behaviour of an Inorganic Passive Film on Hot-Dip Galvanised Steel by Modified Graphene Oxide Incorporation. *Corros. Sci.* **2020**, *174* (January). https://doi.org/10.1016/j.corsci.2020.108846.

(33) Fernández, J.; El Ouardi, Y.; Bonastre, J.; Molina, J. M.; Cases, F. Modification of the Magnesium Corrosion Rate in Physiological Saline 0.9 Wt % NaCl via Chemical and Electrochemical Coating of Reduced Graphene Oxide. *Corros. Sci.* **2019**, *152* (July 2018), 75–81. https://doi.org/10.1016/j.corsci.2019.01.025.

CHAPTER 3. GALVANIC CORROSION INVESTIGATION OF STRUCTURAL TRANSITION JOINTS

3.1. Abstract

Scanning electrochemical microscopy is a useful analysis technique that is increasingly being applied in corrosion and coatings research. In this study, the authors investigated galvanic corrosion properties of an explosively welded iron-aluminum-aluminum alloy clad material called a structural transition joint. Global electrochemical techniques were used to initially identify galvanic activity. The techniques used were open circuit potential, potentiodynamic scanning, and galvanic corrosion current monitoring. Scanning electrochemical microscopy was then applied to sense specific corrosion reactions using a substrate generated/tip collected technique to identify cathodic locations generated from the interfaces of the structural transition joint. Once the galvanic activity was confirmed through scanning electrochemical microscopy, a magnesium sacrificial anode was connected to the joint and tested for its ability to protect the joint from corrosion by passive galvanic protection. Results showed a strong cathodic response to the magnesium anode showing a strong possibility for the joint to be protected by passive galvanic protection.

3.2. Introduction

Structural transition joint (STJ) clad materials are used in maritime ship construction.[1] This joint allows for a strong, welded transition from a steel structure to an aluminum structure.[2] It is comprised of a layer of aluminum 1100 sandwiched between a sheet of SA-516-55 steel and a sheet of aluminum 5086. This three-layer system is created by an explosive welding process. Explosive welding a technique that provides the immense pressure required to fuse the metal sheets together to create the joint utilizing the violent nature of explosives.

The investigation of galvanic corrosion in the structural transition joint is the primary goal of this paper. Galvanic corrosion is the preferential corrosion of a more active metal when two dissimilar metals are electrically connected in a corrosive environment. The active metal corrodes preferentially to the more noble metal causing the active metal's corrosion rate to accelerate while the more noble metal's corrosion rate will decrease. This is primarily observed through an electrochemical cell analysis. The more active metal will show strong anodic activity while the more noble metal will show strong cathodic activity. Significant galvanic interaction is expected between the aluminum and iron in the STJ. The active metal in this case, aluminum, is expected to undergo preferential corrosion at a higher than normal rate while the iron in the steel is expected to be galvanically protected. This galvanic corrosion process could cause the aluminum portion of the material to corrode faster than anticipated causing unexpected structural failure of the joint. However, such preferential galvanic corrosion can be contained and harnessed by protecting the entire joint by the presence of an active metal such as magnesium. With respect to the galvanic series, magnesium is more active than both aluminum and iron. The magnesium would corrode preferentially over the entire joint causing preservation of the joint at the expense of the magnesium sacrificial anode.

Scanning electrochemical microscopy (SECM), introduced by Bard et al in 1989, is a technique and device that can measure local electrochemical reactions.[3–7] A schematic is shown in Figure 3.1 of its configuration. It incorporates local electrochemical monitoring with micro and macro XYZ positioning. The electrochemical reaction occurs through the working electrode in SECM. SECM uses an ultramicroelectrode, UME, as its working electrode. The UME is typically a platinum wire that is encased in a nonconductive shell so that only a finely sanded "disk" is exposed at the tip.

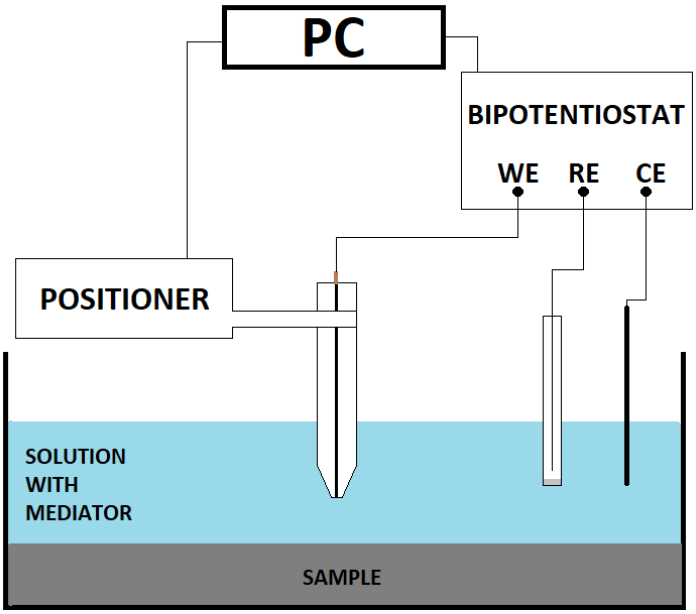

Figure 3.1. Cell configuration of SECM. The three-electrode setup is pictured with a working, reference, and counter electrode.

A conductive solution is used as the medium in which SECM measurements are taken. An electrochemically active chemical within the solution is typically targeted for reduction or oxidation by the UME at the tip. The selectivity of this redox species is controlled through the UME acting as a working electrode while maintaining a selected potential using a potentiostat. The responding tip current created from the redox reaction is then measured by the potentiostat. The current response of an electrochemical reaction facilitated by the UME is dependent on the surface of the material being studied and how it affects the hemispherical diffusion of redox species to the exposed electrode disk. Current from the tip is dependent on (6).[3]

$$i_{\infty} = 4nFDCa \tag{6}$$

In (6), the current is dependent on several variables that are held constant throughout the experiment. The variable, *n*, is the number of electrons transferred, *D* is the diffusion coefficient, *C* is the concentration of the chemical, and *a* is the radius of the UME. This equation holds true

when the electrode is far from the substrate and does not have any negative or positive feedback responses from chemical species.[3,4,8]

The redox chemical used in this study is dissolved oxygen. This method of dissolved oxygen reduction is a commonly used method to monitor corrosive activity.[9–11] In a corrosion cell, dissolved oxygen is reduced at the cathode into hydroxide as shown in (7).

$$O_2 + 2H_2O + 4e^- \rightarrow 4OH^- \quad (7)$$

This reaction consumes dissolved oxygen present near the surface of the cathode. This process creates an area of low oxygen concentration near the surface when compared to bulk concentration. SECM can utilize a redox-competition mode to reduce oxygen at its tip into hydroxide. This allows the UME to act as an "oxygen sensor" by graphing the current while scanning. Areas of high and low current correspond to areas of higher and lower oxygen concentrations respectively.[12–14] Redox-competition mode is attained by the UME reducing a species that is simultaneously being consumed by the surface being analyzed. Areas of low current at the tip would indicate cathodic areas on the sample.

The primary goal of this study is to characterize the corrosion characteristics of a structural transition joint using SECM through oxygen reduction. A secondary objective is to propose the joint be protected through the passive cathodic protection of a magnesium anode.

3.3. Experimental Procedure

The STJ in this investigation consisted of an aluminum alloy sandwiched between an aluminum alloy AA 5086 and steel SA-516-55 Carbon steel. The joint was created via explosive welding process and was provided by NobelClad™ as the product DetaCouple™. The samples were cut laterally such that all three metals/alloys in the joint were exposed during the experimental processes. The STJ was cut and mounted in a mounting epoxy to create a circular

sample that can be mounted in the SECM. As shown in Figure 3.2a, there is an interfacial region between the steel and pure Al. This region contains variable amounts of both Al and steel as well as pitted imperfections all stemming from the manufacturing process. The dynamic material nature of this area is “grey zone” due to the slight shifts in the locations of certain metals. A sample of magnesium was also mounted in the same sample as shown in Figure 3.2b. A wire was soldered to both samples before mounting to allow a switch to be attached to allow galvanic coupling and decoupling of the two metals. The surface of the sample was polished flat with 80 grit and was polished gradually up to 1200 grit using a rotary polisher.

The SECM used in this study was a CHI900b from CH Instruments, Inc. A 10μm UME probe was used with a platinum wire as the working electrode. The counter electrode was platinum, and the reference electrode was Ag/AgCl in saturated KCl. SECM line and area scanning was conducted at a height of 150μm above the substrate.

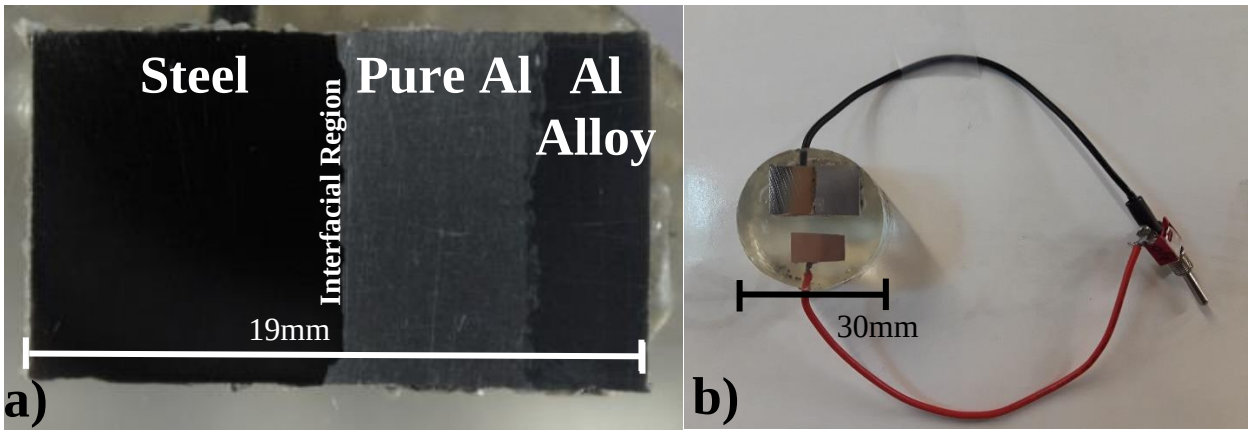

Figure 3.2. a) Magnified image of structural transition joint. The length of the joint is 1.8cm. The composition is SA-516-55 Steel, 1100 aluminum, and 5086 aluminum respectively from left to right. There also exists an interfacial region between the steel and pure Al. b) Entire mounted cell with magnesium to the bottom of the cell. Wires shown with switch for galvanic coupling.

Non-welded samples of the metals used in the joint were also obtained and used for the preliminary global experiments. These experiments were conducted on an Interface 1000 from Gamry Instruments. All global electrochemical experiments used saturated calomel reference

electrodes during testing. Open circuit potential (OCP) was recorded in 3.5% NaCl solution for 1 hour and masked with an insulated tape for an exposed area of $1cm^2$. Immediately following an OCP measurement was a potentiodynamic scan (PDS). The PDS scans were conducted either 1.0V above or below the final OCP measurement. Anodic and cathodic scans of the metals were conducted as separate scans and thus the curve is composed from two separate scans. The scan rate was 1mV/s, and the area was also masked to $1cm^2$. The solution used was 3.5% NaCl in DI water. The galvanic current measurement was conducted with similar parameters as the other two experiments. 3.5% NaCl solution was used, and metals were masked to $1cm^2$. The galvanic current measurement was conducted for 24 hours for each metal pairing.

3.4. Results and Discussion

The first step in this investigation was to identify possible galvanic activity within the joint. The individual metals of the STJ were used to conduct global electrochemical tests such as OCP, PDS, and galvanic current measurement. OCP measurements displayed the range of potential differences of each metal and were measured just prior to the PDS scans as shown in Figure 3.3a and 3.3b. Figure 3.3c displays galvanic current measurements that were administered with the interfaces of the STJ under study. The 1100 aluminum was tested against the 5083 aluminum and the steel. The results showed insignificant current difference between the two aluminum metals but a significant current between the 1100 and the steel, implying strong galvanic interaction between the AA 1100 and Steel 5086.

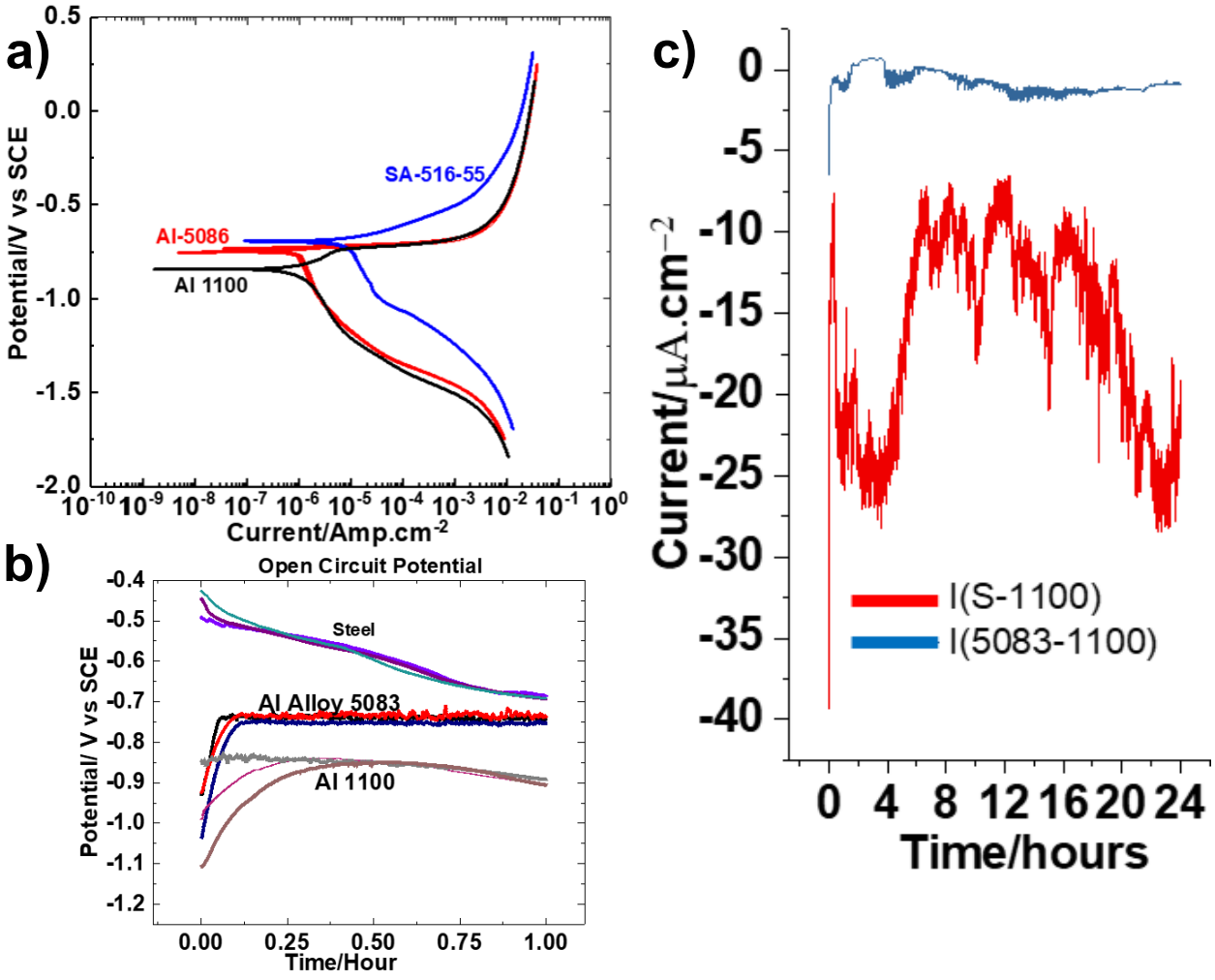

Figure 3.3. Global techniques of individual metals. a) PDS b) OCP c) Galvanic corrosion measurement of interfaces in the joint.

The individual metals were also analyzed with SECM. A redox-competition mode was used to monitor the oxygen concentration above the metal's surfaces. The results, shown in Figure 3.4, detail a baseline of the reactivity with dissolved oxygen in solution. The steel showed great activity along with the aluminum alloy. The pure aluminum showed the least activity.

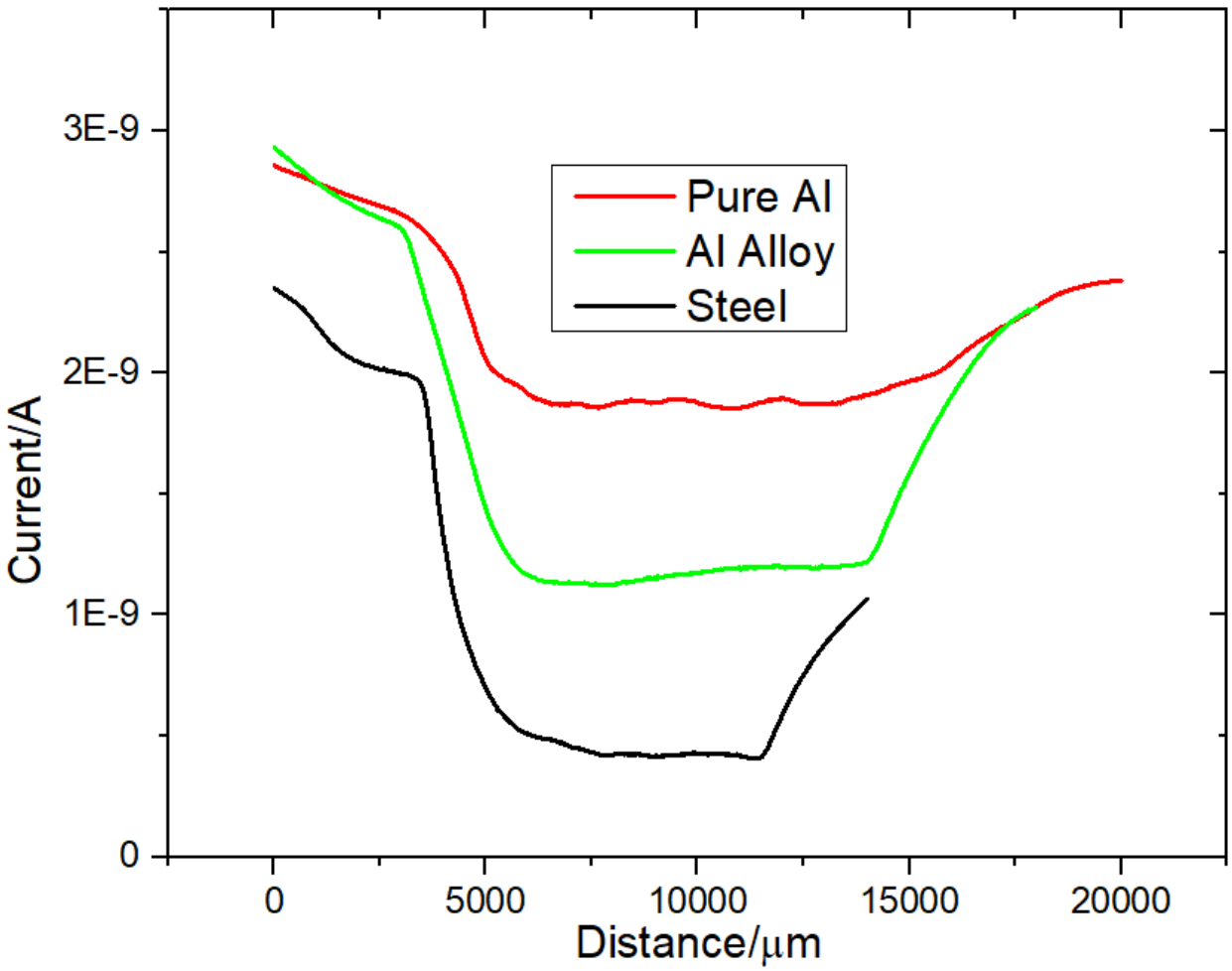

Figure 3.4. SECM line scans of individual metals. The scans were performed 150μm above the surface of the sample with a tip potential of -0.7V vs Ag/AgCl.

Figure 3.5 shows the results of an area scan of the STJ exposed in an epoxy mount. The low current observed over the steel shows that the oxygen concentration is very low. When comparing the observation of the standalone steel sample, the STJ results show lower concentrations of oxygen. This implies that there is an increase in cathodic activity over the steel surface. The pure aluminum shows the largest change in oxygen concentration when comparing Figures 3.4 and 3.5. The STJ results show that oxygen concentration dropped vastly over the pure aluminum location. Based on the galvanic series, aluminum would tend to become anodic

when coupled with steel. If this holds true, then the decrease in oxygen would point to an overall increase in corrosive activity of the pure aluminum.

The aluminum alloy maintained little change when comparing Figures 3.4 and 3.5. This is mostly due to the lack of galvanic activity present between the pure aluminum and the aluminum alloy. This result is also reinforced by the galvanic corrosion results in Figure 3.3c, which shows very little current between the two aluminum types.

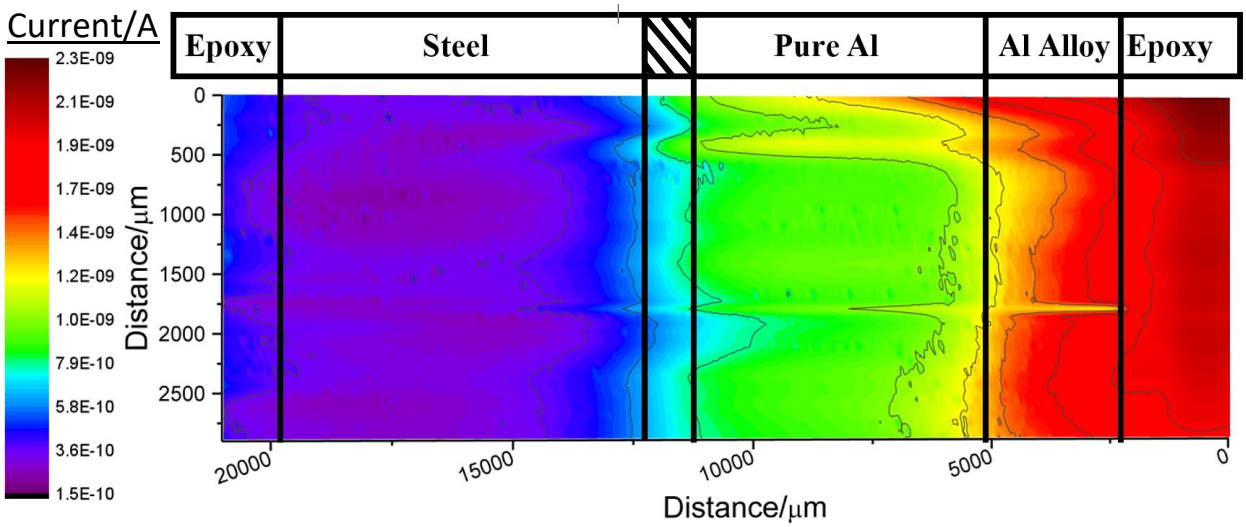

Figure 3.5. Area scan of STJ. The tip potential was -0.7V vs Ag/AgCl at a height of 150μm. The lines on the graph show the locations of the metal transitions over the scanned areas.

The next step was to explore the cathodic protection response of the STJ. Magnesium is a very suitable candidate that is widely used in industry as a sacrificial anode. When coupled with the STJ, the highly active metal should assume highly anodic qualities while the STJ would become more cathodic in nature. As shown previously in Figure 3.2b, the magnesium anode can be connected electrically to the joint using an electrical switch. Figure 3.6 shows a line scan of an uncoupled and coupled sample. The two tests were performed in very close succession to show the dramatic overall decrease in current when connected to the magnesium. This decrease in current shows the decrease in oxygen concentration over the entire STJ. Interestingly, the STJ

holds its general “shape” where the steel is noticeably lower than the aluminum and epoxy surroundings. Both the pure and alloy aluminum exhibit cathodic oxygen concentrations equivalent to the steel levels prior to the magnesium anode. This data points to the joint having a strong possibility to be protected through passive galvanic protection. The signal over the steel portion of the STJ when connected to the Mg anode showed an oxidation current. This is a reversal of the reduction current that was recorded up to now. This oxidation current comes from the rapid H_2 generation on the steel surface. This hydrogen then undergoes oxidation and gives an oxidative current signal.

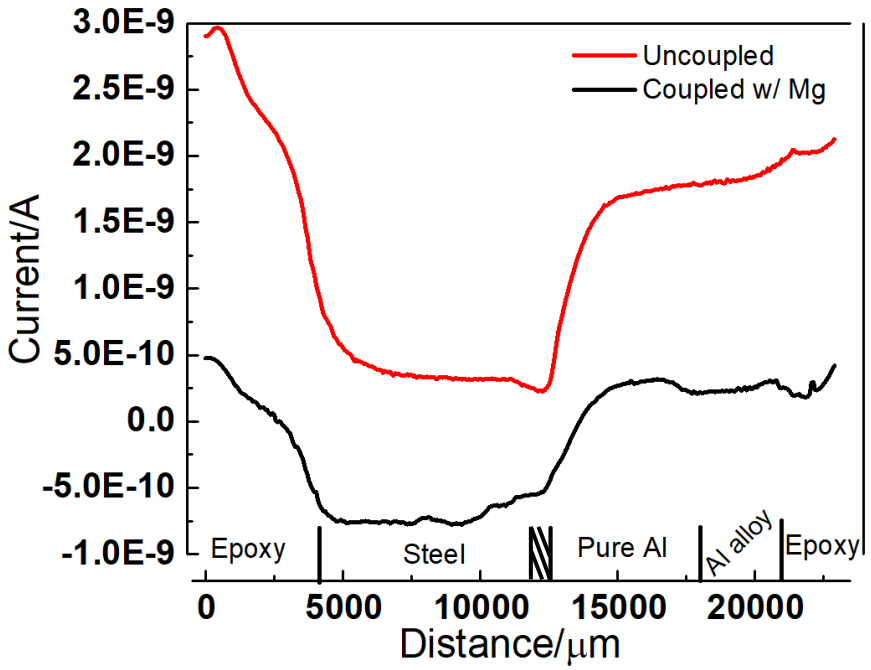

Figure 3.6. Line scans over STJ. Top line represents the uncoupled STJ. Bottom line represents the STJ coupled to magnesium anode. The scan height is 150μm and the tip potential was -0.7V vs Ag/AgCl sat’d KCl.

3.5. Conclusion and Future Work

The study thus far has shown a galvanic presence in the metals, namely the interaction between the steel and pure aluminum interface. SECM was successfully used with redox-competition mode to identify the galvanic presence through oxygen reduction. The results showed that the steel-pure aluminum interface has increased activity. When the magnesium anode was connected to the STJ via wire, SECM was used to analyze the transition of the entire joint to a more cathodic character. This overall increase in cathodic activity over the joint with the Mg anode shows the ability to be cathodically protected for use in marine application.

More experiments are ongoing and are actively pursued for this study. Studies of the effect of acidic and basic pH on the system, coupled and uncoupled, have yet to be interpreted and refined. The use of alternative mediators such as ferrocene-methanol and other redox species such as H^+/H_2 are also in the interest of the study. Other local techniques are also being considered such as SKP. AC-SECM can be applied to analyze the aluminum passive layer while immersed in saltwater.

3.6. References

(1) Ayob, F. Joining of Dissimilar Materials by Diffusion Bonding/Diffusion Welding for Ship Application. *Mar. Front.* **2010**, *1* (9), 69–73.

(2) Liu, W.; Ma, J.; Mazar Atabaki, M.; Kovacevic, R. Joining of Advanced High-Strength Steel to AA 6061 Alloy by Using Fe/Al Structural Transition Joint. *Mater. Des.* **2015**, *68*, 146–157. https://doi.org/10.1016/j.matdes.2014.12.028.

(3) Bard, A. J.; Fan, F. F.; Kwak, J.; Lev, O. Scanning Electrochemical Microscopy. Introduction and Principles. *Anal. Chem.* **1989**, *61* (2), 132–138.

(4) *Scanning Electrochemical Microscopy*, 1st ed.; Bard, A. J., Mirkin, M. V, Eds.; CRC Press: New York, 2001. https://doi.org/10.1201/9780203910771.

(5) Kwak, J.; Bard, A. J. Scanning Electrochemical Microscopy. Theory of the Feedback Mode. *Anal. Chem.* **1989**, *61* (11), 1221–1227.

(6) Bard, A. J.; Fan, F. F.; Pierce, D. T.; Unwin, P. R.; Wipf, D. O.; Zhou, F. Chemical Imaging of Surfaces with the Scanning Electrochemical Microscope. *Science (80-.).* **1991**, *254* (5028), 68–74.

(7) Bard, A. J.; Denuault, G.; Lee, C.; Mandler, D.; Wipf, D. O. Scanning Electrochemical Microscopy: A New Technique for the Characterization and Modification of Surfaces. *Acc. Chem. Res.* **1990**, *23*, 357–363.

(8) Davis, J. M.; Fan, F. R. F.; Bard, A. J. Currents in Thin Layer Electrochemical Cells with Spherical and Conical Electrodes. *Journal of Electroanalytical Chemistry*. 1987, pp 9–31. https://doi.org/10.1016/0022-0728(87)85163-X.

(9) Jamali, S. S.; Moulton, S. E.; Tallman, D. E.; Forsyth, M.; Weber, J.; Wallace, G. G. Applications of Scanning Electrochemical Microscopy (SECM) for Local Characterization of AZ31 Surface during Corrosion in a Buffered Media. *Corros. Sci.* **2014**, *86*, 93–100.

(10) Souto, R. M.; Fernández-Mérida, L.; González, S. SECM Imaging of Interfacial Processes in Defective Organic Coatings Applied on Metallic Substrates Using Oxygen as Redox Mediator. *Electroanalysis* **2009**, *21* (24), 2640–2646.

(11) Santana, J. J.; González-Guzmán, J.; Fernández-Mérida, L.; González, S.; Souto, R. M. Visualization of Local Degradation Processes in Coated Metals by Means of Scanning Electrochemical Microscopy in the Redox Competition Mode. *Electrochim. Acta* **2010**, *55*, 4488–4494. https://doi.org/10.1016/j.electacta.2010.02.091.

(12) González-García, Y.; García, S. J.; Hughes, A. E.; Mol, J. M. C. A Combined Redox-Competition and Negative-Feedback SECM Study of Self-Healing Anticorrosive Coatings. *Electrochem. commun.* **2011**, *13*, 1094–1097.

(13) Jensen, M. B.; Peterson, M. J.; Jadhav, N.; Gelling, V. J. SECM Investigation of Corrosion Inhibition by Tungstate- and Vanadate-Doped Polypyrrole/Aluminum Flake Composite Coatings on AA2024-T3. *Prog. Org. Coatings* **2014**, *77*, 2116–2122.

(14) González-García, Y.; Santana, J. J.; González-Guzmán, J.; Izquierdo, J.; González, S.; Souto, R. M. Scanning Electrochemical Microscopy for the Investigation of Localized Degradation Processes in Coated Metals. *Prog. Org. Coatings* **2010**, *69*, 110–117.

CHAPTER 4. APPLICATION OF MEDIATORS FOR SECM IN THE CORROSION INVESTIGATION OF STRUCTURAL TRANSITION JOINTS

4.1. Abstract

Scanning electrochemical microscopy is a method that incorporates an ultramicroelectrode capable of facilitating electrochemical reactions paired with an XYZ positioning system capable of micron-level movements. This study investigates the corrosion behavior of structural transition joint clad material that contains steel, pure aluminum, and an aluminum alloy blast welded into a single joint. The primary findings of this study center around the application of new mediators and redox-active species for use in corrosion research of SECM such as diquat and ABTS.

4.2. Introduction

Scanning electrochemical microscopy (SECM) is an electrochemical method and device used to analyze surfaces using an ultramicroelectrode (UME) and an XYZ positioning system. The device uses a standard 3-electrode setup for redox reactions. The UME is the working electrode, allowing the user to change the tip potential to target specific reactions. A reference and counter electrode is also used in the apparatus.

A structural transition joint (STJ) is a 3-layer system composed of a top, intermediate, and base layer of Al 5086, Al 1100, and Sa-516-55 carbon steel respectively. This unique material is formed through a process called explosive welding. Explosive welding is the process of using explosives to exert extreme forces on 2 sheets of metal to fuse them together.[1,2] Typically, it is difficult to weld different metals and alloys, but explosive welding allows this type of material to be manufactured. The primary use for a STJ is shipbuilding. The joint allows a transition of a steel hull to the aluminum superstructure.[1,3]

There are two novel mediators used in this study to analyze the corrosion of the STJ. One is diquat dibromide monohydrate (diquat), and the other is 2,2'-azino-bis(3-ethylbenzothiazoline-6-sulfonic acid) diammonium salt (ABTS). Diquat was typically used as an herbicide and used in the agriculture industry before glyphosate was introduced.[4] Diquat and ABTS have been found to have meditative properties with iron ions.[5] Diquat can be reduced to produce a radical form that will reduce Fe^{+3} to Fe^{+2} and form a positive feedback with sufficient Fe^{+3} concentrations. Similarly, ABTS can be oxidized to produce a radical that will oxidize Fe^{+2} to Fe^{+3} forming a similar positive feedback with sufficient Fe^{+2} concentrations.[5] Figure 4.1 gives a visual representation of the mediation processes.

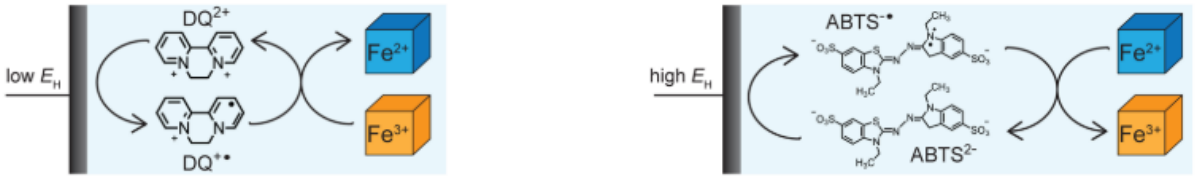

Figure 4.1. Electrochemical mediation of diquat and ABTS with iron ions.[5]

4.3. Experimental Outline

All SECM experiments were conducted with solutions prepared with 3.5% NaCl w/w in DI water. A 3.5% NaCl solution was used for all solutions to maintain conductivity and reactivity of the STJ throughout the experiments. A 3mM solution of analytical grade diquat dibromide monohydrate (diquat) obtained from MilliporeSigma was prepared. A 1mM solution of >98% 2,2'-azino-bis(3-ethylbenzothiazoline-6-sulfonic acid) diammonium salt (ABTS) obtained from MilliporeSigma was prepared. A third solution of 1% w/w NaI obtained from MilliporeSigma was also prepared. All SECM experiments utilized a Ag/AgCl(sat'd KCl) for a reference electrode and a platinum wire as a counter electrode. The model of SECM was a

CHI900b from CH Instruments, Inc. The SECM is contained within a double-walled grounded Faraday cage.

The STJ was obtained from NobelClad and mechanically cut to size. Samples were created to expose the interfacial face of the joint. The joint was mounted in epoxy, sanded, and polished to a mirror finish. A magnesium anode was electrically connected to the joint prior to mounting in epoxy. This anode is connected via a switch to allow the circuit to open or close between the joint and the Mg anode. The use of the Mg is for its possibility as a sacrificial anode. Passive galvanic protection is a process that utilizes the preferential corrosion of paired metals to the advantage of the target material. A sacrificial anode, such as Mg, will corrode preferentially over a less active metals such as Fe. This process can be used to protect certain structures from corrosion and materials while replacing the rapidly corroding anode when needed.

4.4. Results and Discussion

The primary focus of this study was to characterize the corrosion behavior of a STJ using new and previously studied mediators and methods with SECM. By comparing and contrasting the results of different mediators under similar corrosion conditions, we can begin to construct a characterization of the STJ that encompasses the many "strengths" of each mediator when applied to corrosion studying.

Iron ion oxidation has been used before in SECM to analyze a scribe in a coating healing.[6] Iron ion oxidation has also been used in the characterization of stainless steel corrosion.[7–9] These studies applied an oxidation potential to the UME and would oxidize Fe^{+2} originating from the anode of iron corrosion and oxidize it further into Fe^{+3}.[9] The mode that the SECM would operate in for this kind of iron ion oxidation would be substrate-generated/tip-collected(SG/TC).

The first scans performed over the STJ are shown in Figure 4.2. Peaks that are present without Mg show areas of Fe^{+2} generating from the surface. These spikes are caused by steel corrosion. There are notably two locations of prominent iron corrosion: the left-most edge of the STJ away from any Al and at the interface between the steel and the pure Al. The corrosion near the edge of the joint is mostly likely caused by a typical corrosion process that any steel when placed in a corrosive environment might encounter. The Al has a lot of iron mass and surface area between the observed corrosion and the interface. Galvanic effects could be minimized at this distance, allowing the far edge of the steel to undergo uniform corrosion. The other area of note is the right near the interface between the steel and the pure Al. This area is closest to the pure Al. Because of the strong galvanic corrosion potential between Fe and Al, this area would seem to be the most "protected" by the pure Al corroding due to its close proximity to the pure Al. There exists the pits and imperfections in the steel-pure Al interface which could allow steel corrosion to occur.

The scan was then repeated with the Mg couple engaged to allow the Mg anode to enter the galvanic interaction. Here we observed an increase in current across the entire surface of the steel. However, this is not from Fe^{+2} oxidation. The connection of the Mg anode causes large amounts of H_2 generation on the STJ and most so on the steel portion. These rapidly generated bubbles are saturating the solution at the surface with H_2. H_2 is easily oxidized into H^+ with the tip potential of +0.5V vs Ag/AgCl(sat'd KCl) which is the potential of the UME for these tests.[10]

Both scans exhibited little activity over the Al portions of the joint. With a slight increase with the Mg anode most likely from a small amount of H_2 generation.

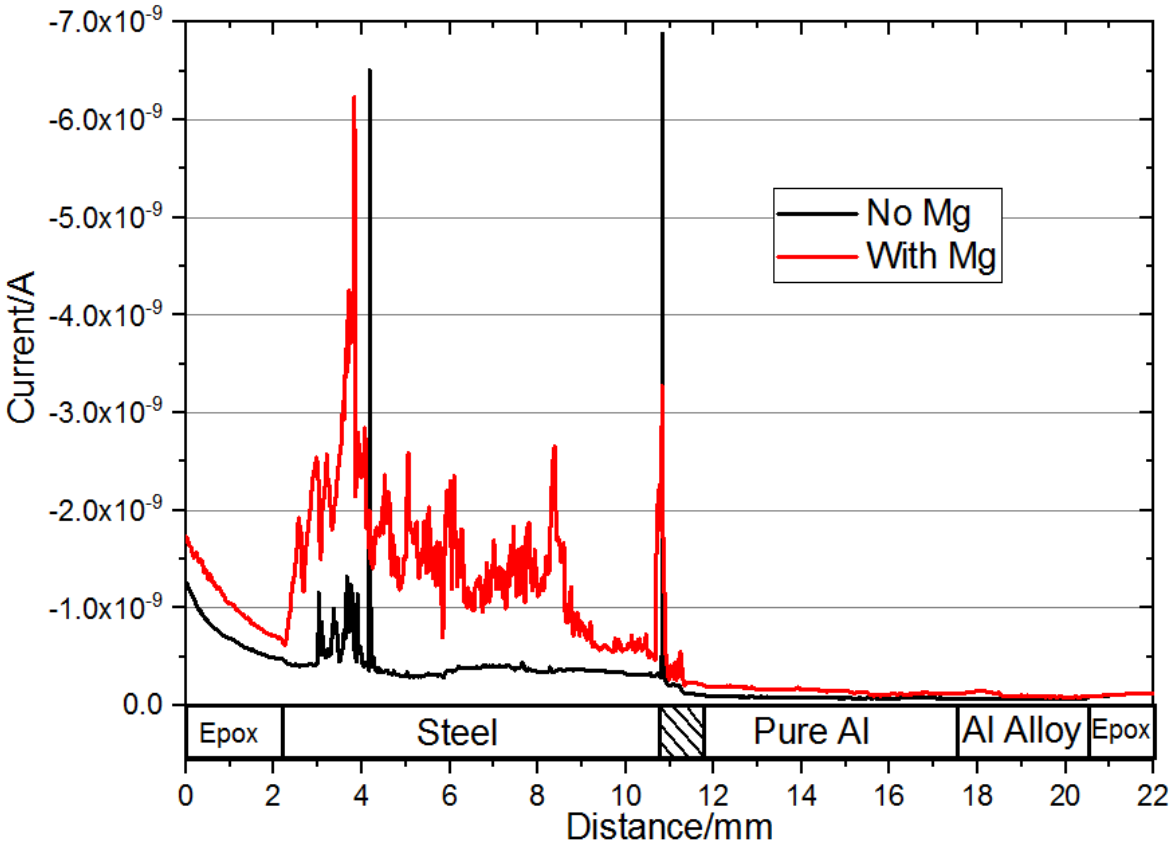

Figure 4.2. SECM lines scan at +0.5V vs Ag/AgCl(sat'd KCl). The scan height was 20µm. The solution was 3.5% NaCl w/w in DI water.

Figure 4.3 displays the results of diquat being used as the mediator with SECM. Figure 4.3 displays two graphs of the same scan surface and settings, except Figure 4.3(B) is on a larger current scale because Figure 4.3(A) maximized the current for that current range. Without the Mg anode, there are small oxidation peaks over the edge of the steel/epoxy interface and the steel/pure Al interface. There appears to be little activity throughout, and no reduction current observed over the STJ. We did observe a green hue to the solution immediately above the steel portion of the STJ. This hue is caused by the generation of the radical form of diquat, which has a green color. As shown in Figure 4.1, the UME reduces the diquat into its radical form which will reduce Fe^{+3}. The cathode could carry out the reaction of the supplied electrons radicalizing the diquat. This effectively removes any mediator for the UME to reduce. This explains the near-

zero current shown over the steel portion, effectively converting the SG/TC mode we were using into a redox-competition mode.

When the galvanic couple was created with the STJ, a large oxidation peak was recorded over the steel portion. There is also increased current over both the pure-Al and Al alloy portions of the STJ. The large spikes are most likely caused by H_2 oxidation similarly to Figure 4.2. The cathode typically causes a higher pH due to the generation of OH^-. This can allow H_2 to be oxidized by the reduction potential of -0.55V vs Ag/AgCl used in this experiment. An interesting observation arises from the magnitude of the oxidation current. This current is, on average, 2 orders of magnitude higher than the H_2 oxidation recorded during Fe^{+2} oxidation in Figure 4.2. There must be additional oxidation reactions occurring with the presence of diquat to causes this increase in current that is caused by the high cathodic activity on the steel portion.

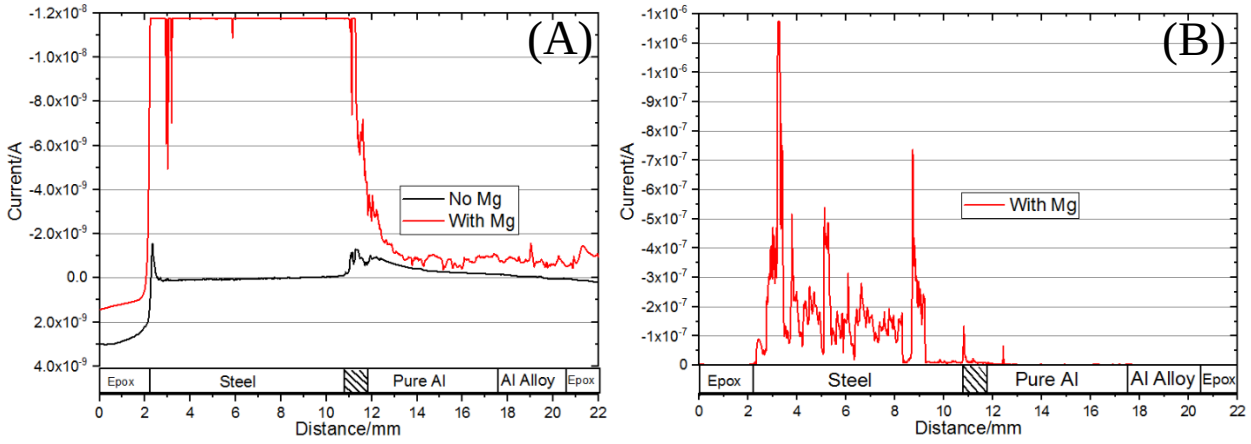

Figure 4.3. SECM line scan at -0.55V vs Ag/AgCl(sat'd KCl). The graph (A) is on a scale of 10^{-9} while (B) is a duplicate scan with Mg on the scale of 10^{-7} due to the current limit reached on (A). The tip height was 20µm. The solution was 3mM diquat dibromide in 3.5% NaCl w/w solution.

Figure 4.4 displays the results of ABTS mediation. As shown in Figure 4.1, ABTS has the opposite mechanism as diquat. The ABTS radical formed at the UME oxidizes Fe^{+2} to Fe^{+3}. It would be reasonable to assume that the results would be near identical to the Fe^{+2} oxidation in

Figure 4.2. This holds true for scanning over the steel portion without the Mg anode. There are oxidation peaks observed over the Al portions of the STJ without the Mg anode. These readings could be an interaction of the ABTS with generated species originating from the anodic Al portions. When the Mg anode is connected, we observe the H_2 oxidation current seen previously throughout the STJ. The primary differences observed between the Fe^{+2} oxidation and ABTS mediation is the increased activity over the Al portions of the STJ. Fe^{+2} oxidation showed little to no signal over the Al portions while the ABTS mediation displayed an oxidation current without the Mg anode and a slightly decreased oxidation current with the Mg anode.

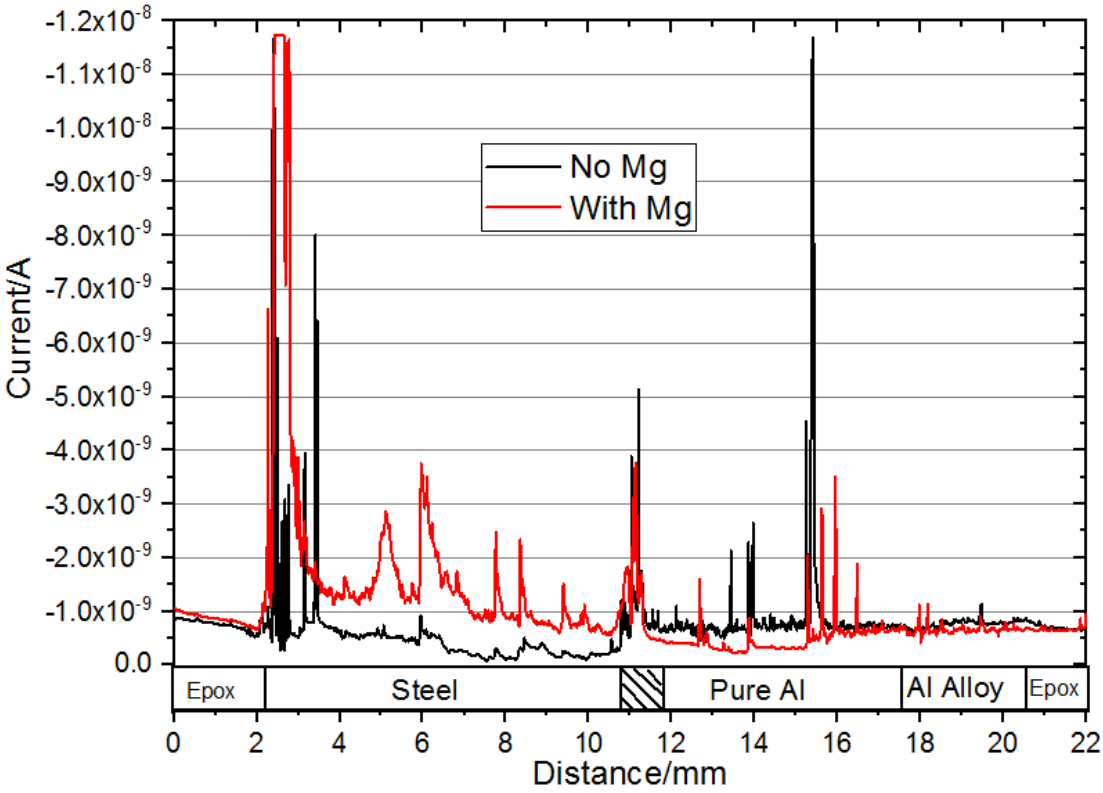

Figure 4.4. SECM line scans at +0.6V vs Ag/AgCl(sat'd KCl). The tip height was 20µm. The solution was 1mM ABTS in 3.5% NaCl w/w solution.

Figure 4.5 displays the SECM results of I^- mediation. Iodine mediation operates in SG/TC mode by oxidizing $3I^-$ into I_3^-.[7,11] The generated I_3^- then oxidizes Fe^{+2} into Fe^{+3}.[7] Theoretically, this creates a similar SG/TC mode as Fe^{+2} oxidation and ABTS mediation. We

would expect to see the presence of Fe^{+2} oxidation peaks above anodes and H_2 oxidation peaks during high cathodic activity. In Figure 4.5, (A) displays the results of the I^- mediation, while (B) shows a spike recorded at higher current capacity when scanning with the Mg couple.

Without the Mg couple, the current responded with a dip in oxidation current on the steel edge as shown in Figure 4.5(A). The current drops over the steel portion as it gets closer to the pure Al interface. It then spikes over the interface and increases to bulk-currents ranges over the rest of the STJ. The dip in current could be an adsorption of iodine onto the steel surface. The Fe^{+2} oxidation peaks are missing in this graph. In past experiments, the steel substrates have had to be polarized with an oxidation potential for I^- mediation to proceed.[7,11] I^- mediation could possibly not be sensitive enough to detect Fe^{+2} oxidation in the parameters used in this experiment. With the Mg anode, the I^- couple has a large current response over the steel edge. The current drops considerably over the rest of the steel and increases to a steady level over the Al portions of the STJ. The I^- mediation current feedback appears to be hindered by cathodic activity which is shown to a greater extent when the STJ is coupled with the Mg anode. The cathode must consume the I^-, possibly through adsorption onto the surface of the STJ or by an interaction with the cathode reactions. By this presumption, it would appear that there is very little cathodic activity above the Al alloy as well as most of the pure Al near the pure Al-Al alloy interface without the Mg anode.

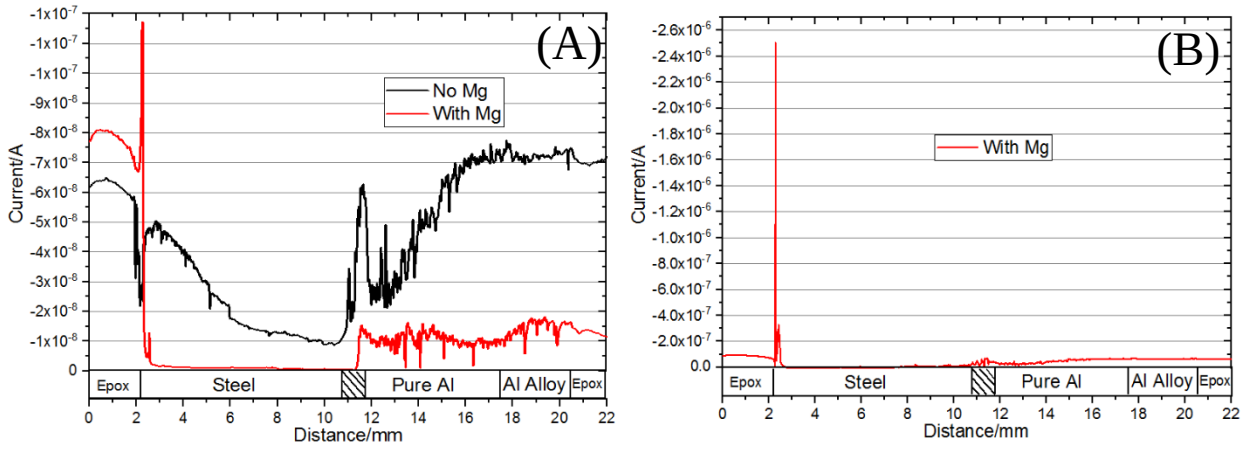

Figure 4.5. SECM line scans at +0.6V vs Ag/AgCl(sat'd KCl). Graph (A) displays on the scale of 10^{-8} while graph (B) displays on the scale of 10^{-6}. The tip height was 20µm. The solution was 1%NaI w/w in 3.5% NaCl w/w solution.

4.5. Conclusions

The purpose of this study was to expand upon the corrosion characterization of structural transition joints using new mediators as well as expanding upon developing mediator methods using scanning electrochemical microscopy. The work shown in this study showed the amperometric responses to changes in mediator concentrations over the metal portions of the structural transition joint as well as positive feedback current responses. Fe^{+2} oxidation displayed the anodic locations over the steel portion of the joint and that, despite the galvanic couple, there is iron undergoing oxidation despite the galvanic interaction with the Al portions. The same scan also displayed no oxidizable species present in solution over the Al portions of the joint. I^- mediation a strong response to cathodic activity and little current response to anodic areas. Two new redox chemicals were used with SECM: ABTS and diquat. Diquat scans with SECM displayed little activity when the STJ was isolated. No Fe^{+3} ion presence was observed from the diquat mediation. There displayed some peaks around the edge of the steel portion as well as the steel-pure Al interface, but this was observed as an oxidation current and could not be a result of diquat mediation. This was overshadowed by the results gathered from the attachment of the Mg

anode. The resulting activity throughout the STJ showed that diquat exhibits strong oxidation current characteristics in the presence of strong cathodic activity in parallel with H_2 oxidation. ABTS results matched similar peaks as Fe^{+2} moderation which is expected due to the oxidation potential used for ABTS mediation, but little evidence of mediation was observed due to the oxidation current levels being almost identical in scale to unmediated Fe^{+2} oxidation. There existed many peaks identified over the Al portions of the STJ that ABTS reacted to in small sharp peaks. This activity held through the attachment of the Mg anode and was consistent with and without the anode. This activity could point to an interaction with the anodic activity that is present above the pure-Al.

4.6. References

(1) Ayob, F. Joining of Dissimilar Materials by Diffusion Bonding/Diffusion Welding for Ship Application. *Mar. Front.* **2010**, *1* (9), 69–73.

(2) Chen, X.; Inao, D.; Tanaka, S.; Mori, A.; Li, X.; Hokamoto, K. Explosive Welding of Al Alloys and High Strength Duplex Stainless Steel by Controlling Energetic Conditions. *J. Manuf. Process.* **2020**, *58* (July), 1318–1333. https://doi.org/10.1016/j.jmapro.2020.09.037.

(3) Liu, W.; Ma, J.; Mazar Atabaki, M.; Kovacevic, R. Joining of Advanced High-Strength Steel to AA 6061 Alloy by Using Fe/Al Structural Transition Joint. *Mater. Des.* **2015**, *68*, 146–157. https://doi.org/10.1016/j.matdes.2014.12.028.

(4) Abu Shawish, H. M.; Ghalwa, N. A.; Hamada, M.; Basheer, A. H. Modified Carbon Paste Electrode for Potentiometric Determination of Diquat Dibromide Pesticide in Water and Urine Samples. *Mater. Sci. Eng. C* **2012**, *32* (2), 140–145. https://doi.org/10.1016/j.msec.2011.10.008.

(5) Sander, M.; Hofstetter, T. B.; Gorski, C. A. Electrochemical Analyses of Redox-Active Iron Minerals: A Review of Nonmediated and Mediated Approaches. *Environ. Sci. Technol.* **2015**, *49* (10), 5862–5878. https://doi.org/10.1021/acs.est.5b00006.

(6) Pilbáth, A.; Szabó, T.; Telegdi, J.; Nyikos, L. SECM Study of Steel Corrosion under Scratched Microencapsulated Epoxy Resin. *Prog. Org. Coatings* **2012**, *75*, 480–485.

(7) Yin, Y.; Niu, L.; Lu, M.; Guo, W.; Chen, S. In Situ Characterization of Localized Corrosion of Stainless Steel by Scanning Electrochemical Microscope. *Appl. Surf. Sci.* **2009**, *255*, 9193–9199.

(8) Casillas, N. Scanning Electrochemical Microscopy of Precursor Sites for Pitting Corrosion on Titanium. *J. Electrochem. Soc.* **1993**, *140* (9), L142. https://doi.org/10.1149/1.2220897.

(9) González-García, Y.; Burstein, G. T.; González, S.; Souto, R. M. Imaging Metastable Pits on Austenitic Stainless Steel in Situ at the Open-Circuit Corrosion Potential. *Electrochem. commun.* **2004**, *6*, 637–642.

(10) Zhou, J.; Zu, Y.; Bard, A. J. Scanning Electrochemical Microscopy - Part 39. The Proton/Hydrogen Mediator System and Its Application to the Study of the Electrocatalysis of Hydrogen Oxidation. *J. Electroanal. Chem.* **2000**, *491* (1–2), 22–29. https://doi.org/10.1016/S0022-0728(00)00100-5.

(11) Lister, T. E.; Pinhero, P. J. The Effect of Localized Electric Fields on the Detection of Dissolved Sulfur Species from Type 304 Stainless Steel Using Scanning Electrochemical Microscopy. *Electrochim. Acta* **2003**, *48* (17), 2371–2378. https://doi.org/10.1016/S0013-4686(03)00228-7.

CHAPTER 5. CHARACTERIZATION OF HIGH-TEMPERATURE COATINGS TREATED AT DIFFERENT TEMPERATURES

5.1. Abstract

High-temperature coatings, designed to be used at a wide range of temperatures, find many applications in industries. However, there still lacks a good understanding of how these coatings change during their service at very high temperatures. In this study, we characterize several commercial high-temperature coatings exposed to different levels of heat. General trends of decreasing barrier performance were observed with the exception when these coatings are exposed to their rated temperature limit of 1400°F, at which the barrier increased slightly, indicated by their low-frequency impedance modulus. To further investigate this "phenomenon", we characterize the coatings with infrared spectroscopy, thermogravimetric analysis, scanning electrochemical microscopy, and energy-dispersive X-ray spectroscopy. The results showed that both the substrate surface oxidation and pyrolyzed coating binder are both contributing factors of the increase in barrier performance of samples exposed to 1400°F.

5.2. Introduction

High-temperature coatings are coatings that are designed to maintain barrier performance up to temperatures that are much higher than environmental conditions. These types of coatings find application in the energy sector, high-heat piping, and other applications that require metal protection under high temperatures. High-temperature coatings can also find specific use in the prevention of corrosion-under-insulation. The binder that is commonly used in coatings of high-temperature application is silicone. A more formal name for silicone is polysiloxane. Polysiloxane is made up of a repeating pattern of Si-O bonds. This polymer backbone is commonly functionalized with organic groups to increase its thermal stability and is well-studied

for its high-temperature applications.[1–4] The addition of phenyl groups have been shown to increase thermal stability on polysiloxane chains and have led to the specialization of high-temperature applications.[5–7]

Metals that undergo high temperatures typically form what is known as scale. Scaling is the uniform oxidation of a metals surface to form a layer of metal oxide. This layer is typically fragile and has weak adhesion to the metal. In some stainless steels, scaling can lead to a protective layer from corrosion due to the composition and stability of the formed scale.[8] Many factors of the environment can shape and decide the nature of the scale formed on a metals surface.[8–11]

The coatings described in this study hold a certification under the performance standard of MIL-PRF-14105E at the time of the publishing of this study. MIL-PRF-14105E describes the performance standard of a single-coated, single component, heat-resistant coating. The primary goal of this standard is to describe a coating that can undergo heat to a maximum of 1400°F (760°C). The standard describes the required compositional standards of the coating to either be Type I or Type II. The primary difference between types is the VOC content. Type I describes a coating with VOC content maximum of 3.5 lbs/gal, and Type II describes the VOC content maximum of 2.8 lbs/gal.[12] The coatings tested in this study fall into either Type I or Type II. MIL-PRF-14105E is important for this study since the report describes the expected performance standards for a certified coating. This study centers around corrosion resistance and barrier performance described within the standard. MIL-PRF-14105E describes heating a coating to different temperatures and perform different testing to measure any possible performance degradation due to high temperatures. These standards were used as a template in the testing performed in this study.

A common technique used to evaluate coating performance is electrochemical impedance spectroscopy (EIS). The method involves applying a small AC signal to the substrate and measuring the resulting current. Coatings have inherent resistance and capacitive qualities with how an AC signal is measured through the coating. This method is commonly used to evaluate coating performance and is regarded as a standard testing of barrier performance.[13–20] The primary method for barrier performance centers around low-frequency impedance measurements. Low frequency (0.01Hz) impedance gives a measure of the barrier performance of a coating.[21–23]

5.3. Experimental Outline

The primary objective of this study was to investigate the coating performance changes of coatings that were heated to 1400°F.

5.3.1. Materials

The three coatings that were investigated in this study all hold the certification of mIL-PRF-14105E. Coating 1 is manufactured by The Sherwin Williams Company and is named C71B6. Coating 2 is manufactured by Hentzen Coatings, Inc. and is named 02308KML-HF. Coating 3 is manufactured by NCP Coatings, Inc. and is named N-9455. In EIS measurements, a 3.5% NaCl (w/w) solutions was used as a conductive solution. A room-temperature ionic liquid was also used in the substrate testing with EIS and PDS in addition to the salt solution. The ionic liquid was 1-butyl-1-methylpyrrolidinium trifluoromethanesulfonate.

5.3.2. Panel Preparation

Cold-rolled steel panels were obtained from GPI that fit the requirements of MIL-PRF-14105E. The dimensions were 6” x 3” x 3/16”. These panels were then sand blasted to SSPC-

SP5 standard by the manufacturer prior to shipping. Panels were then cleaned with acetone in accordance with SSPC-SP1 prior to coating.

Each of the 3 coatings used in this study had manufacturer recommended application instructions with wet film thicknesses ranging from 3-5 mil. Every paint was mixed for at least 30 minutes, maintaining a vortex prior to application. Air spray was used as the application method of each coating. These coatings were then allowed 24 hours to air dry followed by a 1-hour cure at 400°F.

B117 accelerated weathering was conducted on coated panels as described in ASTM B117. Panels were under exposure for 100 hours.

5.3.3. Heating Regimen

Once panels were coated and cured. Panels were then selected to undergo various levels of heat exposure. All panels were heated for 1 hour in an oven at 400°F and then heated to a specific temperature as displayed in Table 1. Heating panels to 400°F to fully cure was specified by all manufacturers of the three coatings. The temperatures selected were 650°F, 800°F, 1000°F, and 1400°F. Panels heated to 400°F only were used as the control for comparisons made to other exposed panels. Once panels were heated to their respectful temperatures for 1 hour, they were taken out of the kiln and allowed to air cool to room temperature.

Table 5.1. Heating regimen for 15 coated panels. All oven temperatures at sample insertion were room temperature except the 800°F panels were inserted into a 650°F oven and then brought up to 800°F for the 1-hour heat exposure.

Oven Temperature(°F)	400	650	800	1000	1400
Panel # involved	1-15	4-6	7-9	10-12	13-15

5.3.4. Thin Film Creation

For TGA and FT-IR Spectroscopy analysis, thin films were created using glass panels and a drawdown bar set to 4 mil of wet film thickness. These samples were heated in the same manner as the steel-substrate panels resulting in samples of the temperature ranges of 400°F, 650°F, 800°F, 1000°F, and 1400°F. The resulting films were then removed from the glass panels with a razor, resulting in powders to be used for analysis.

5.3.5. Thermogravimetric Analysis (TGA)

The powders underwent TGA from the ranges of room temperature to ~1500°F with a scan rate of 68°F per minute. The weight of the powders was recorded during that time and compared to the original starting weight. The sample had a constant rate of 50mL/min of nitrogen gas to avoid atmospheric influence. The device used was a Q500 TGA from TA Instruments.

5.3.6. Differential Scanning Calorimetry (DSC)

Thin-film powders were also analyzed under differential scanning calorimetry (DSC). The samples were massed and tared from their containers and analyzed in a Q1000 DSC from TA Instruments. The samples were analyzed through a heat/cool/heat regimen. The 2nd heating ramp was analyzed for any transitions of the coating. The coating was heated to 400°C at 20°C/min in the initial ramp then cooled at 10°C/min to 0°C. The samples were then heated at 20°C/min to 400°C while the heat flow was being measured. A constant gas flush of 50mL/min of nitrogen gas was used to avoid any atmospheric influence.

5.3.7. FT-IR Spectroscopy

Each of the powders underwent FT-IR Spectroscopy with the intent of identifying the molecular degradation of the coating as the exposure temperature was increased. The samples

were scanned from 650 to 4000 wavenumber and the reflectance was recorded. A Thermo Scientific Nicolet 8700 Fourier Transform Infrared Spectrometer was used for all samples.

5.3.8. Electrochemical Impedance Spectroscopy (EIS)

Coated steel panels were subjected to several EIS measurements before and after 100 hours of B117. Three samples of every heating level underwent this test-B117-test cycle. Two samples were scribed with an "X" while the other one was left untouched for accurate EIS testing. The scribing was performed after heating but before weathering. Visual comparison between all samples were performed in accordance with MIL-PRF-14105E.

EIS was performed with potentiostats in a sealed faraday cage to avoid EM noise. A 3-electrode setup was used with 3.5% NaCl solutions used as the dominant solution. A room-temperature ionic liquid was also. The reference electrode was a Ag/AgCl in saturated KCl reference. The counter used was a platinum mesh. The samples were masked to have an exposure of 1 cm^2. With a new area scanned for every test. The frequency range began at 100,000Hz and ended at 0.01Hz with a perturbation of 10mV RMS.

5.3.9. Potentiodynamic Scanning (PDS), and Substrate Testing

Uncoated substrates were evaluated using EIS and PDS. PDS describes a linear potential scan from negative of the OCP of the metal to the positive side. The intent is to have the open circuit potential lie in the path of the scan to form a curve that describes both anodic and cathodic activity of the tested metal. The PDS testing scanned +/-0.5 volt from open circuit potential, measured for 1 hour prior to testing. Scanning was performed from cathodic to anodic at a scan rate of 5mV/s. The exposed surface area was 1 cm^2 and a Ag/AgCl sat'd KCl reference electrode was used throughout testing. The device used for both PDS and EIS measurements was a Gamry Instruments Interface 1000 Potentiostat. PDS testing was performed separately with 3.5% NaCl

and 1-Butyl-1-methylpyrrolidinium trifluoromethanesulfonate, a room temperature ionic liquid (RTIL). The RTIL allows a electrochemical test to be conductive without the presence of corrosive medium such as salt water. The room temperature ionic liquid has a conductivity of 1.85 mS/cm. This conductivity is adequate to mitigate the contribution of solution resistance towards the testing.

5.3.10. Scanning Electron Microscopy (SEM) and Energy-dispersive X-ray Spectroscopy (EDS)

Samples were prepared by cutting small cross-sectional pieces approximately 1x1 cm and polishing the interface with sandpaper. These were then further polished with an argon-ion beam prior to imaging.

5.4. Results and Discussion

The initial testing involved the accelerated weathering process described in B117. Pictures were taken of each set of panels before and after 100 hours of B117. A visual comparison of before and after weathering was made. The pictures are displayed in Figure 5.1. All 3 coatings showed large amounts of corrosion product as well as coating failure throughout the temperature ranges. Coating 1 and Coating 3 showed visually an improvement in performance in the 1400°F samples when compared to the panels of the same coating exposed to lower temperatures. The samples had less blistering and a decrease in corrosion product throughout the panel barring the scribe. This is an unexpected observation since heat typically degrades a coating and performance would decrease.

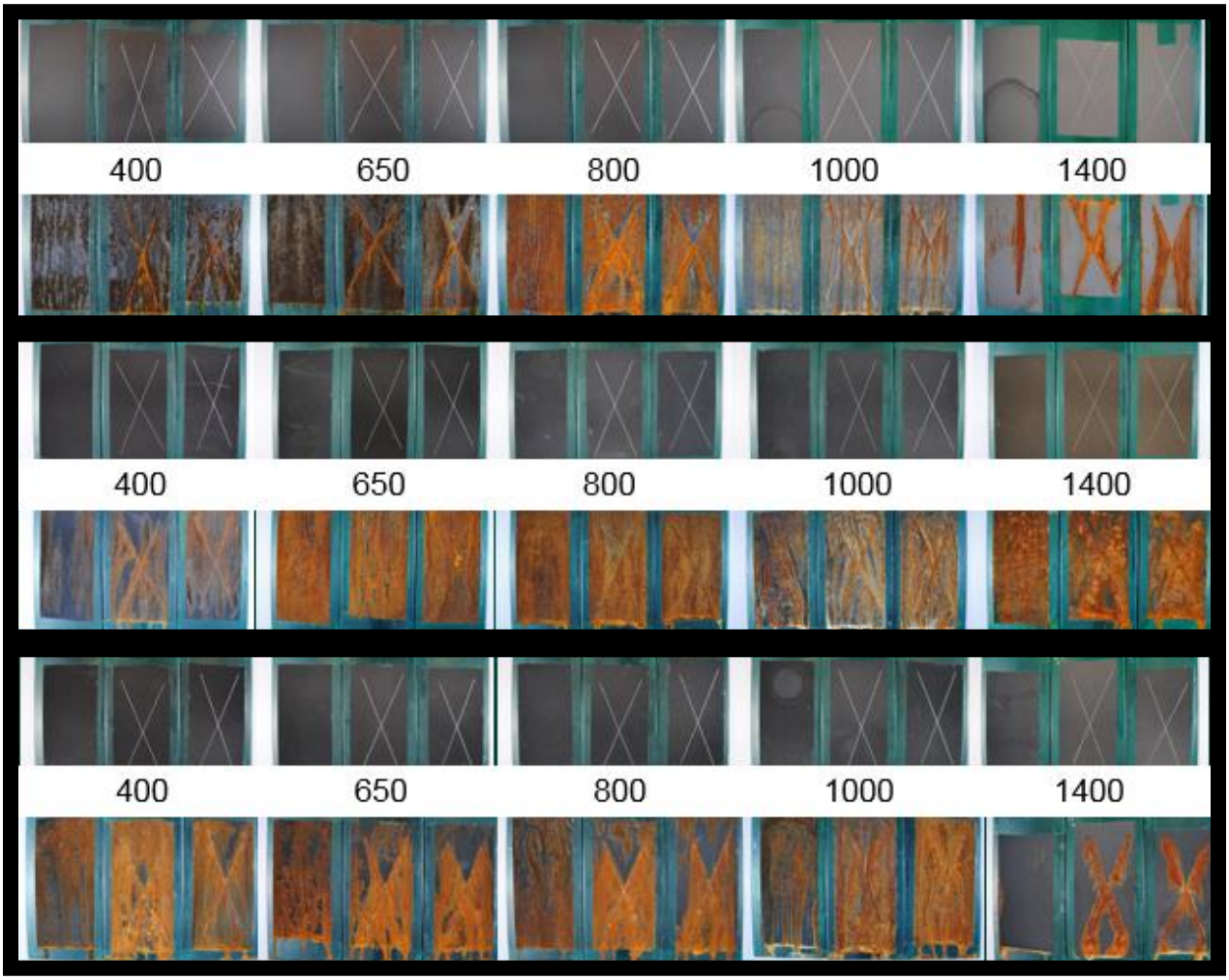

Figure 5.1. Photos taken of all B117 samples before and after 100 hours of accelerated weathering. The order of panels is Coating 3(top), Coating 2(middle), and Coating 1(bottom). The panels above the temperature exposure are prior the accelerated weathering with the after pictures located below. Note: some before pictures show the residual moisture of EIS testing.

The results of EIS are shown in Figure 5.2. A general trend of decreasing performance as the temperature increased. This is what is expected. Thermal degradation of a coating causes physical voids, tears, and other damage to a coating. This is then recorded through EIS as low impedance. Every coating tested has comparable barrier performance at 1000°F to bare substrate. Interestingly, all samples show an increase in barrier performance after this at the 1400°F level. This consistent increase in barrier performance could be caused by a reaction or physical change that all the coatings undergo past 1000°F to cause the coating barrier to “repair” in some way.

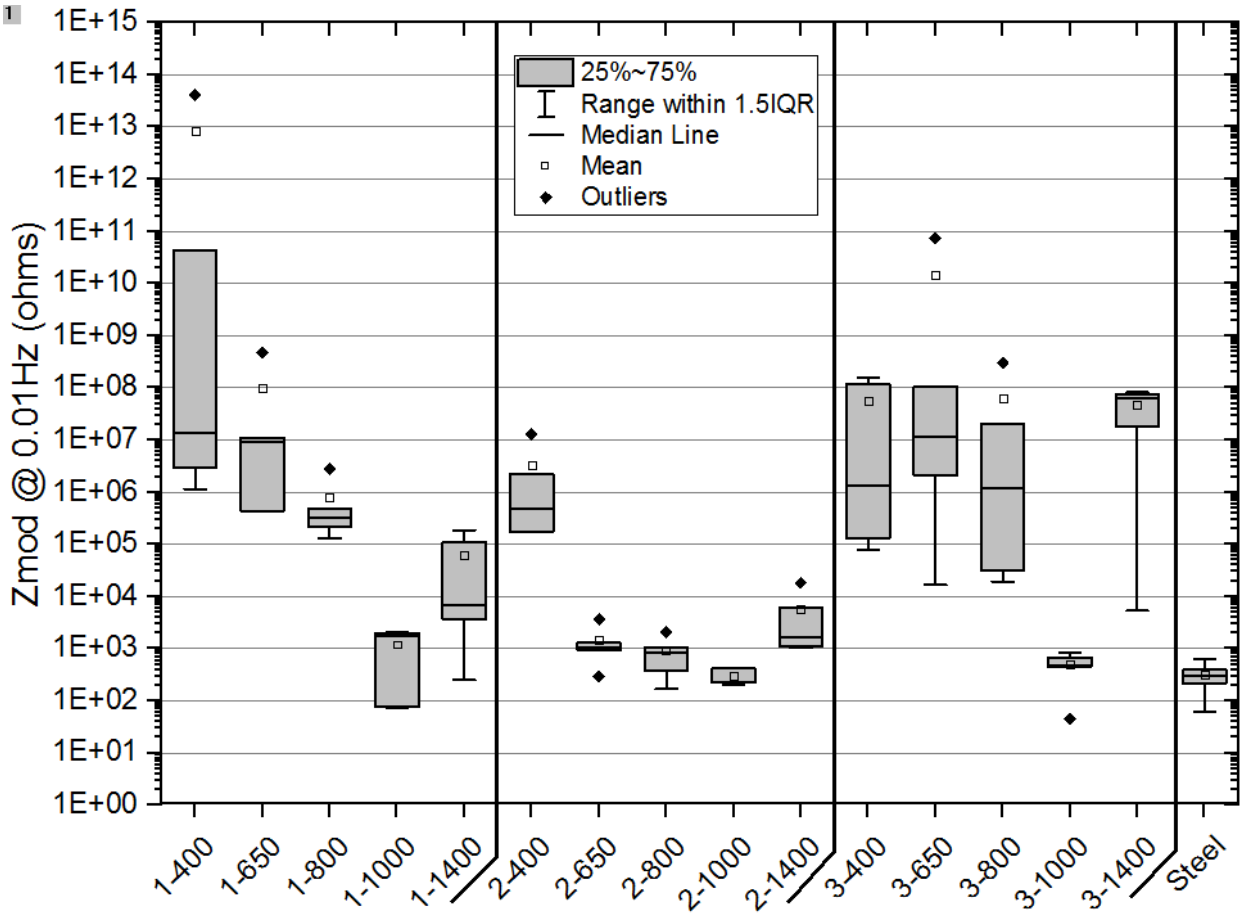

Figure 5.2. EIS data of all 3 coatings. The data displayed is the impedance of the coatings at low (0.01Hz) frequency. The area of the scanned area was 1 cm^2. The first number is the coating followed by the temperature level (e.g., "2-650" is equivalent to "Coating 2 heated to 650°F") At least 5 replicates of each coating were performed.

TGA was used to observe thermal breakdown of the coating through mass loss. Figure 5.1 shows the results of the 3 coatings undergoing TGA. MIL-PRF-14105E gives the maximum operating temperature at 760°C (1400°F). Heating to 800°C surpasses this standard and is used as the maximum in the tests. As shown in Figure 5.3, all 3 coatings showed similar mass loss up to 275°C (527°F). Coating 1 retained most of the original mass with 88% of its remaining mass present at 800°C. Coating 3 and 2 had 84% and 70% remaining at the end respectively. The high amounts of original mass remaining show the temperature-resistance of the substances used in these coatings. Despite this, the formulations still contain volatile materials at such high

temperatures in either different amounts or compositions. Based off the visual inspection after B117, Coating 2 performed the worst at 1400°F. The TGA results show that Coating 2 loses much more mass compared to Coatings 1 and 3. The decrease in protective coating mass could be a factor in the low performance of Coating 2.

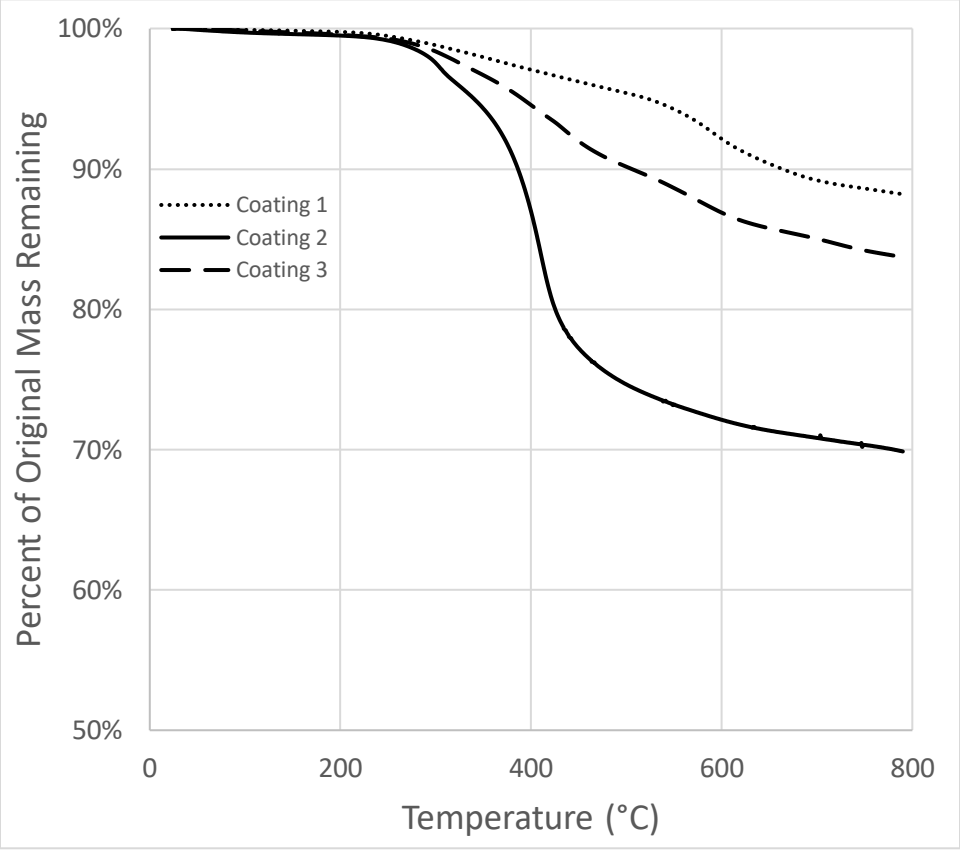

Figure 5.3. TGA results of 3 coatings cured at 400°F. Coatings were heated from room temperature to 800°C at a rate of 20°C/min.

The results of DSC testing are shown in Figure 5.4. The primary purpose of DSC testing was to identify any transitions such as glass transition, crystallization, or melting. These could then be compared to films that were heated to different temperatures. What is most notable about Figure 5.4 is the complete lack of transitions. DSC data typically stems from the polymer behavior as it is heated as transitions in the polymer causes changes in heat flow. The suspected polymer either has little transition characteristics or has already deteriorated. Another option is

that the polymer is so heavily crosslinked that there is no molecular maneuverability to cause transitions that can be affected at these temperatures.

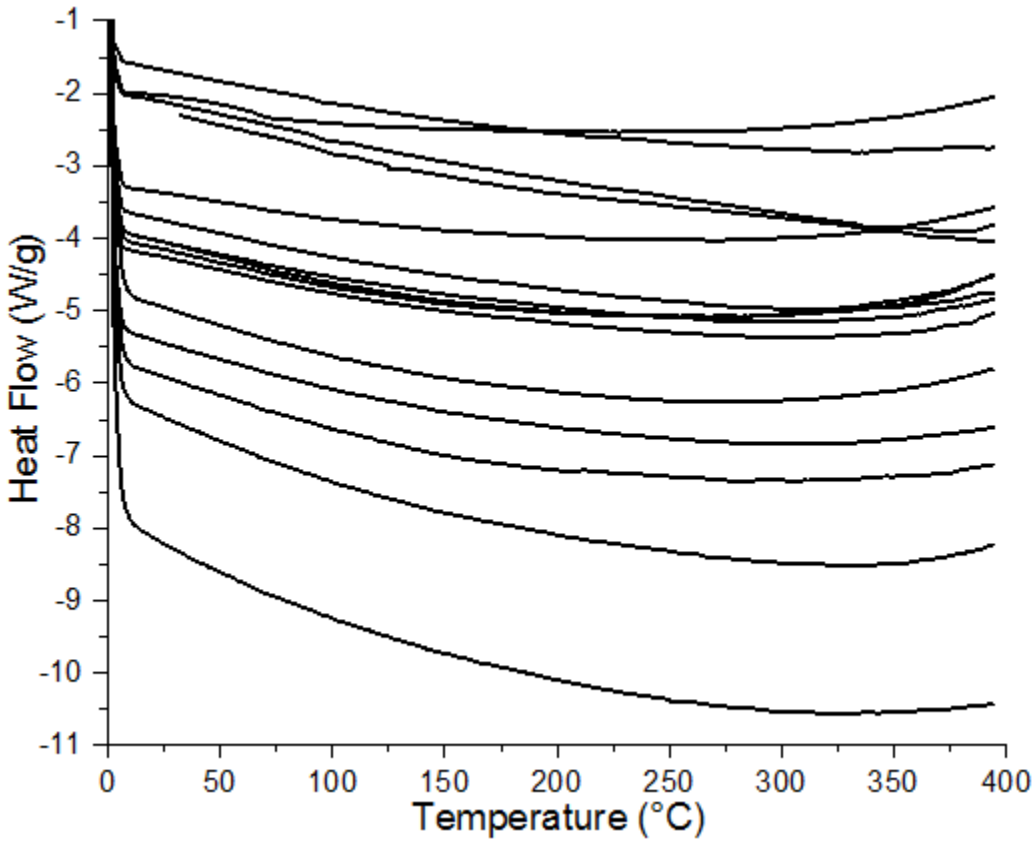

Figure 5.4. DSC Results. Individual samples were not labeled since all results yielded no transitions.

FTIR was used to identify possible composition of the coatings to find either a degradation or creation of certain compounds which may affect the effectiveness of a coating might have regarding corrosion prevention or as a barrier. Each coating was exposed to different heating levels and the FT-IR spectrum of those results were recorded and shown in Figures 5.5-5.7 of Coatings 1,2, and 3 respectively. Overall, silicon-based binders were observed across every coating. It was concluded that every coating contained a silicone backbone with functional groups being composed of phenyl or methyl groups. Poly(diphenylsiloxane),

poly(methylphenylsiloxane), poly(dimethylsiloxane), and intermediate derivatives have been studied before for their temperature-resistance.

Past 800°F, peaks that denote these silicone peaks mostly disappear and little to no peaks become discernable. This is mainly due to the breakdown of most of the silicone into its decomposed forms such as oxides. Organosilicon-based FT-IR spectroscopy always has a large broad peak centered approximately from 1000 to 1100 wavenumber.[24] This peak hides a lot of SiO_2 peaks which could be the product of the backbone decomposing.

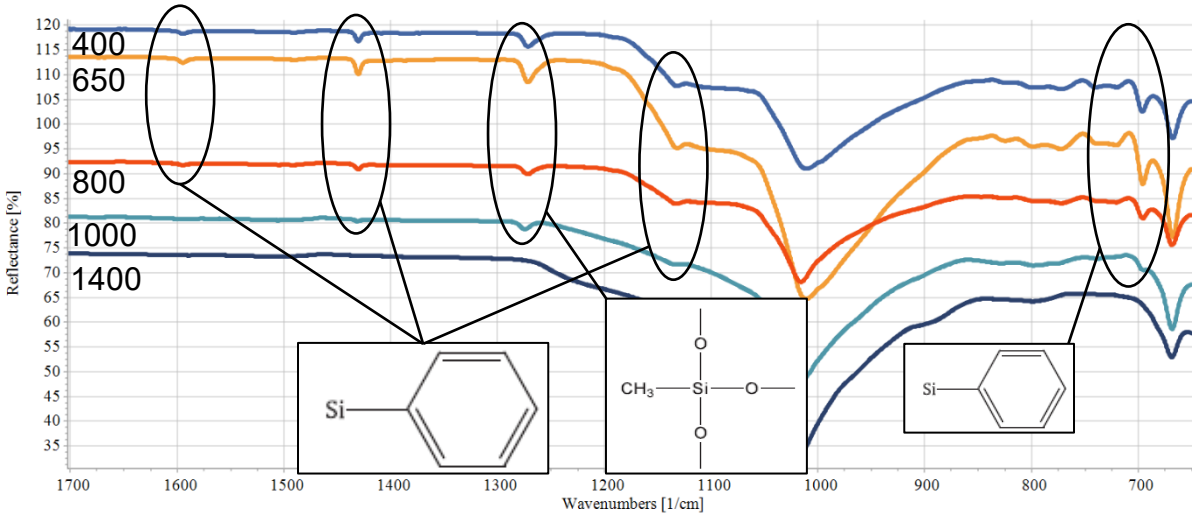

Figure 5.5. FT-IR Results of Coating 1. Y-axis is shifted for visual-comparison purposes and does not represent the actual reflectance values.

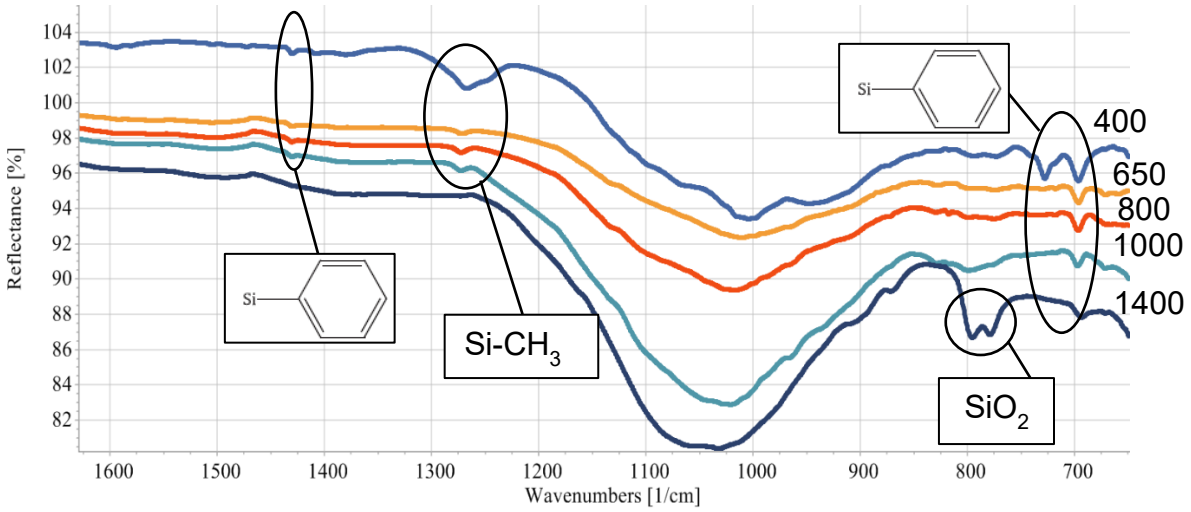

Figure 5.6. FT-IR Results of Coating 2. Y-axis is shifted for visual-comparison purposes and does not represent the actual reflectance values.

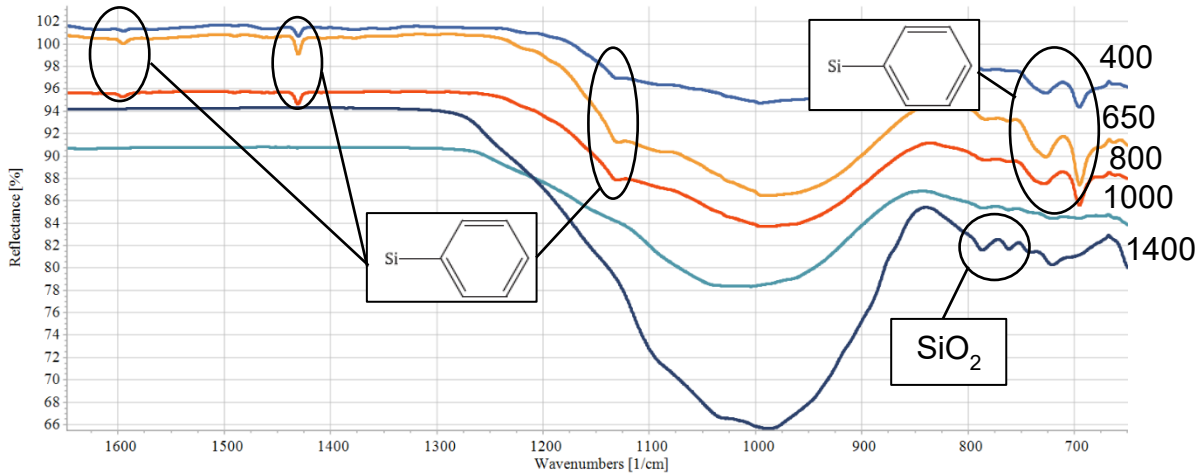

Figure 5.7. FT-IR Results of Coating 3. Y-axis is shifted for visual-comparison purposes and does not represent the actual reflectance values.

SEM was used in this study to visually inspect the physical micro-structures of a cross-section of the substrate and coating after undergoing the heating regimen. EDS was also utilized to identify elements present in the different physical features identified in SEM to evaluate possible chemical changes that happen within the system as a whole. The results of both scanning electron microscopy imaging and energy-dispersive X-ray spectroscopy composition scanning of samples are shown in Figures 5.8-5.10. A single coating was evaluated for this

portion of testing, Coating 1. The 1-800, 1-1000, and 1-1400 panels were analyzed due to the transitional performance that we observe between these samples. These samples were not weathered prior to the imaging and X-ray analysis.

The lighter bottom half of each image is the steel substrate with the coating appearing in the top half of the image. Observations from the pictures show that in the 1-1400 images, there is a gap between the coating and the substrate. This gap is not present in the other two samples (1-800 and 1-1000) despite undergoing the same polishing regimen and having the same coating. While the polishing regimen was consistent throughout the 3 samples to expose this edge, one cannot rule out that this gap is caused by it. Conversely, this gap is unique and well defined throughout the 1-1400 sample. The increased temperature might have had an effect in creating this, either through an incompatibly in thermal expansion of materials or unstable scaling of the steel substrate.

Energy-dispersive X-ray spectroscopy, or EDS, is a method to gather data about the elemental composition of a very fine point. This is useful when paired with SEM. EDS samples were taken of numerous points in the samples. The results gave feedback on what elements are present at those locations. Using this data, we can postulate different molecules that make up the composition of the interface.

In the 1-800 and 1-1000 samples, most composition measurements show signs of inorganic pigments dispersed in a silicon binder. This is as expected of a typical coating. Figure 5.8 shows a thin line that acts as an interface between the steel and the coating. This is a film of most likely iron oxide. High amounts of iron and oxygen are measured on this interlayer. It is likely that this layer was present prior to coating due to natural oxidation from the atmosphere.

With regards to the 1-1400 sample in Figure 5.10, the gap shows interesting results. The gap showed is not between the steel and the coating. Pure steel substrate makes up the “ceiling” of the gap with iron oxide making up the “floor”. This means that a micron-scale layer of steel is separating from the rest of the substrate. This layer, if consistent with the other coatings’ physical structures, could be an insulating layer that is causing increased barrier performance readings through EIS. This additional separation with a non-conductive iron oxide layer could cause increased impedance and causing improved barrier performance.

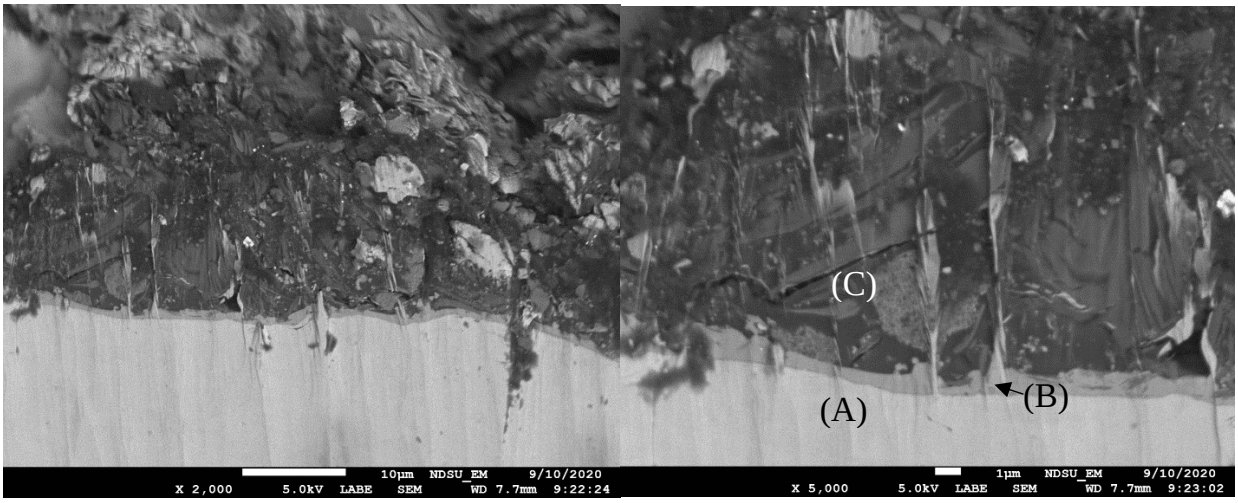

Figure 5.8. SEM pictures of 1-800.EDS location results: (A) Steel substrate; (B) Iron oxide, trace silicon; (C) Silicon binder, inorganic pigments.

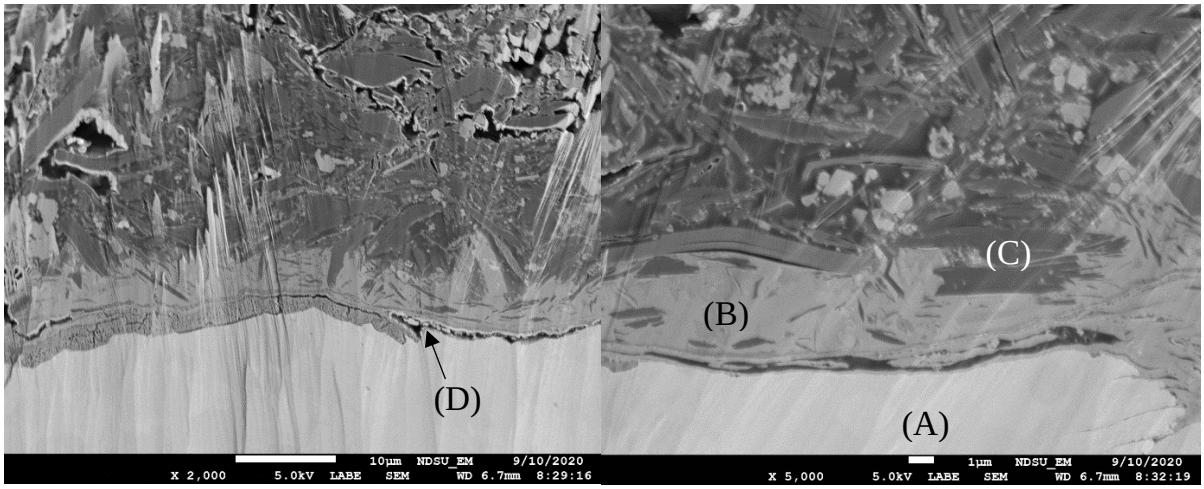

Figure 5.9. SEM pictures of 1-1000. EDS location results: (A) Steel substrate; (B) Iron oxide, inorganic pigments; (C) Silicon binder, inorganic pigments; (D) Void.

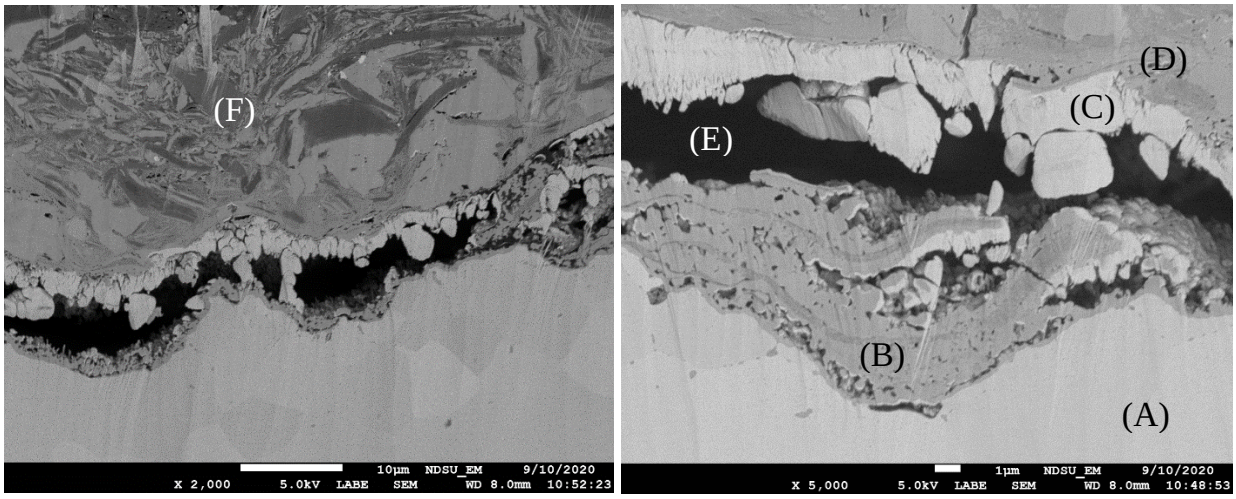

Figure 5.10. SEM pictures of 1-1400. EDS location results: (A) Steel substrate; (B) iron oxide; (C) Steel substrate; (D) Iron oxide, trace pigments and silicon; (E) Void; (F) silicon binder, inorganic pigments.

The phenomenon described in this paper could be due to the substrate developing a protective layer due to the heat. Bare, uncoated substrate underwent the heating regimen and then EIS was performed on the different heat levels. Initially, the 1000°F and 1400°F samples developed a flaky layer that released from the substrate to reveal an unaffected substrate underneath. The EIS results obtained from this method gave consistent impedance comparable to the control. The heating regimen was repeated with particular care and haste to move the panels

from the oven to a desiccator as quickly as possible to avoid any effect oxygen may have on the substrate during cooling. This worked by preserving any oxidation layers from flaking off and maintaining adhesion to the substrate. The results are shown in Figure 5.11. EIS was performed with two solutions. A 3.5% NaCl and a room-temperature ionic liquid (RTIL) was used as the solution for the two sets of scans. The use of these two liquids allows us to evaluate the impedance in both. The use of the RTIL was to be able to perform both EIS and PDS while maintaining the fragile nature of the scaling. The ions and corrosive nature of the 3.5%NaCl salt solution could affect the scaling.

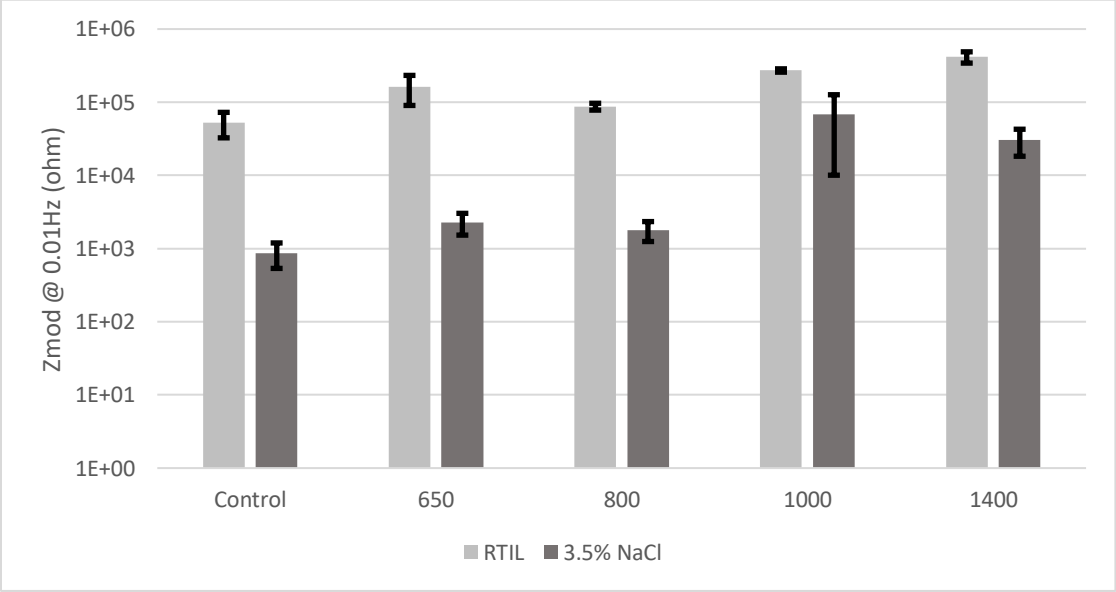

Figure 5.11. EIS results of substrate testing at low frequency.

The results of Figure 5.11 show a slight increase in barrier performance in the 1000°F and 1400°F panels, particularly in the 3.5% NaCl solution. The 1400°F bare steel panels show similar performance as Coating 1 and 2 at 1400°F. The performance increase of the 1000°F steel panel shows better performance than the lower temperatures. When compared to the coated 1000°F panels, the 1000°F bare steel panels show better performance. This is not expected since any coating, even degraded, would only add to the performance as a barrier.

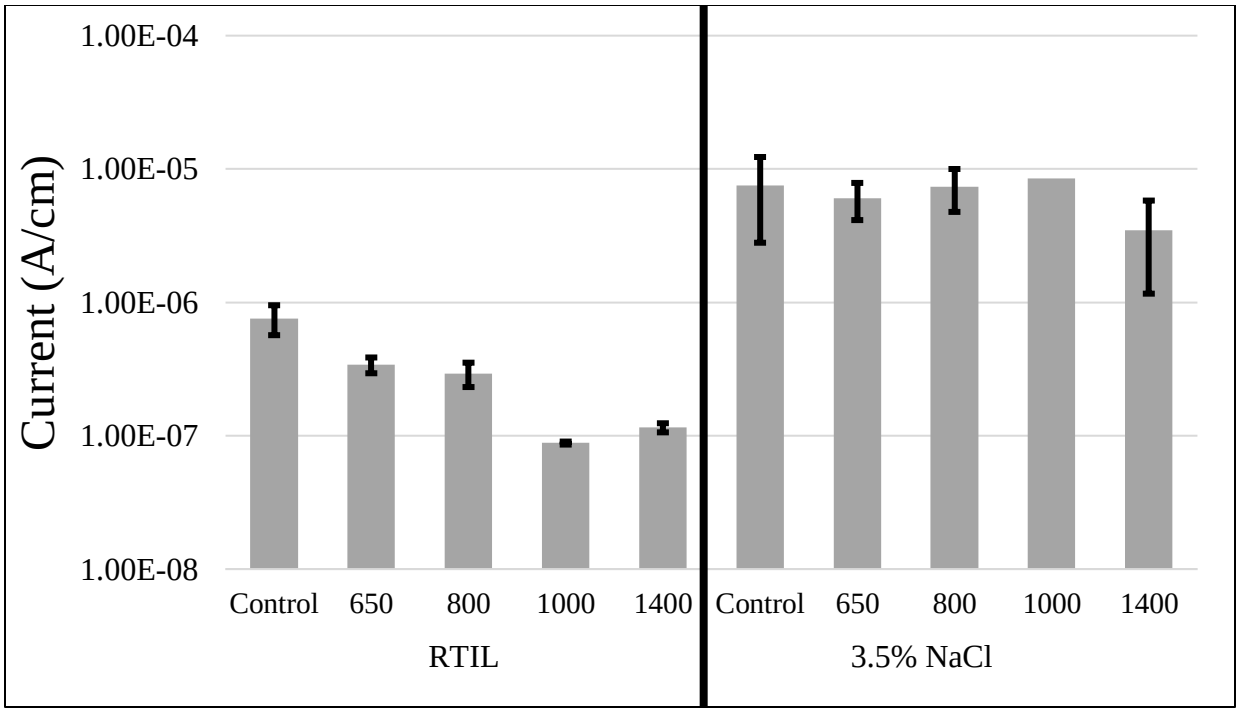

Figure 5.12. Corrosion current (I_{corr}) results attained from PDS Scans. The area scanned was $1cm^2$. A lower value is a smaller corrosion rate.

The results of the PDS reinforce the EIS bare substrate observation. The PDS results are displayed in Figure 5.12. The RTIL results showed decreased current in the 1000°F and 1400°F samples when compared to the lower temperature panels. This decrease in current is linked to decreased corrosion. The 3.5% NaCl showed similar results with the 1400°F bare steel showing a strong resistance to polarization, indicating corrosion resistance.

The reason for the increased performance of 1000°F and 1400°F is the creation of a protective oxide layer. Oxide layers have the ability to maintain stability and cohesiveness when formed under the correct conditions. The higher temperatures may create the right environment for this oxide layer to form which could act as a barrier to corrosion.[9,10,25]

400°F	– Coatings reach manufacturer-recommended curing temperature. Coatings' performances are maximized.
650°F	– All coatings begin experiencing mass loss due to decomposition. Coatings 1 and 2 experience a substantial performance loss.
800°F	– Coating 2 has lost ~25% of its mass by this level. Coatings 1 and 3 have loss less than 10% of their original mass. Coating 3 has sustained their coating performance at acceptable levels up to this point. Coatings 1 and 2 show slightly worst performance than at 650°F. Most signatures of the polymer binder have maintained stability up to this point.
1000°F	– All coatings experience barrier performance measurements on par with a bare, unheated substrate. All coatings display minimal protection of the substrate. Polymer structure is unstable and decomposing into inorganic oxides. Voids near the substrate surface begin forming. Iron oxide from the substrate and inorganics from the polymer begin incorporating on the substrate/coating interface. Bare substrates begin showing a noticeable increase in corrosion resistance and barrier performance.
1400°F	– Most signals of polymer binder have disappeared from measurements. Mass loss is minimal as temperature increases past this point. Barrier performance rises with coating 3 reaching impedance higher than at 400°F levels in locations on the test panel. Signatures of SiO_2 display in FT-IR spectroscopy. Voids are present throughout under the surface of the substrate and iron oxide forms inside the void. Iron oxide has increasingly incorporated with the coating. Bare substrates show similar performance to the 1000°F levels of heating.

Figure 5.13. Mechanism explanation at each heating level.

5.5. Conclusion

The results of this study show a measurable increase in coating performance when heated to 1400°F. The coatings all contain a polysiloxane that breaks down at or above 1000°F to form decomposition products. These products either chemically or physically change the coating to act

as a barrier to both increase impedance and to resist corrosion. In parallel to this process, the steel substrate is creating oxide layers that are providing protection on par with the coated samples heated to the same temperature. The combined processes are causing a performance increase that was measured primarily with low-frequency EIS impedance measurements alongside many supporting testing methods.

5.6. References

(1) Deshpande, G.; Rezac, M. E.; Irisawa, T. The Effect of Phenyl Content on the Degradation of Poly(Dimethyl Diphenyl) Siloxane Copolymers. *Polym. Degrad. Stab.* **2001**, *74* (2), 363–370. https://doi.org/10.1016/S0141-3910(01)00186-0.

(2) Wang, H. F.; Zhao, X. G.; Liu, X. C.; Chen, L.; Wang, L. F.; Chen, C. H.; Wu, Z. W. Synthesis and Thermal Properties of PEEK-PEDEK Block Copolymers. *Gaodeng Xuexiao Huaxue Xuebao/Chemical J. Chinese Univ.* **2004**, *25* (6), 1156.

(3) Lee, M. K.; Meier, D. J. Synthesis and Properties of Diarylsiloxane and (Aryl/Methyl)Siloxane Polymers: 1. Thermal Properties. *Polymer (Guildf).* **1993**, *34* (23), 4882–4892. https://doi.org/10.1016/0032-3861(93)90013-Z.

(4) Patil, R. D.; Mark, J. E. Evaluations of Forcefields for Aromatic Polysiloxanes, and Some Applications to Poly(Diphenylsiloxane). *Comput. Theor. Polym. Sci.* **2000**, *10* (1–2), 189–195. https://doi.org/10.1016/S1089-3156(99)00079-3.

(5) Israeli, Y.; Lacoste, J.; Cavezzan, J.; Lemaire, J. Photooxidation of Polydimethylsiloxane Oils and Resins. IV-Effect of Phenyl Groups. *Polym. Degrad. Stab.* **1995**, *47* (3), 357–362. https://doi.org/10.1016/0141-3910(94)00128-6.

(6) Ogliani, E.; Yu, L.; Mazurek, P.; Skov, A. L. Designing Reliable Silicone Elastomers for High-Temperature Applications. *Polym. Degrad. Stab.* **2018**, *157*, 175–180. https://doi.org/10.1016/j.polymdegradstab.2018.10.012.

(7) Hamdani, S.; Longuet, C.; Perrin, D.; Lopez-cuesta, J. M.; Ganachaud, F. Flame Retardancy of Silicone-Based Materials. *Polym. Degrad. Stab.* **2009**, *94* (4), 465–495. https://doi.org/10.1016/j.polymdegradstab.2008.11.019.

(8) Asteman, H.; Svensson, J. E.; Johansson, L. G. Evidence for Chromium Evaporation Influencing the Oxidation of 304L: The Effect of Temperature and Flow Rate. *Oxid. Met.* **2002**, *57* (3–4), 193–216. https://doi.org/10.1023/A:1014877600235.

(9) Samal, S. High-Temperature Oxidation of Metals. In *High Temperature Corrosion*; InTech, 2016; Vol. 524, pp 141–157. https://doi.org/10.5772/63000.

(10) Chen, R. Y.; Yuen, W. Y. D. Study of the Scale Structure of Hot-Rolled Steel Strip by Simulated Coiling and Cooling. *Oxid. Met.* **2000**, *53* (5), 539–560. https://doi.org/10.1023/a:1004637127231.

(11) Sun, W.; Tieu, A. K.; Jiang, Z.; Zhu, H.; Lu, C. Oxide Scales Growth of Low-Carbon Steel at High Temperatures. *J. Mater. Process. Technol.* **2004**, *155–156* (1–3), 1300–1306. https://doi.org/10.1016/j.jmatprotec.2004.04.172.

(12) PAINT, HEAT-RESISTING (FOR STEEL SURFACES), MIL-PRF-14105E. 2011, pp 1–16.

(13) Wolstenholme, J. Electrochemical Methods of Assessing the Corrosion of Painted Metals-a Review. *Corros. Sci.* **1973**, *13* (7), 521–530. https://doi.org/10.1016/S0010-938X(73)80002-2.

(14) Margarit-Mattos, I. C. P. EIS and Organic Coatings Performance: Revisiting Some Key Points. *Electrochim. Acta* **2020**, *354*, 136725. https://doi.org/10.1016/j.electacta.2020.136725.

(15) Suay, J. J.; Rodríguez, M. T.; Razzaq, K. A.; Carpio, J. J.; Saura, J. J. The Evaluation of Anticorrosive Automotive Epoxy Coatings by Means of Electrochemical Impedance Spectroscopy. *Prog. Org. Coatings* **2003**, *46* (2), 121–129. https://doi.org/10.1016/S0300-9440(02)00219-9.

(16) Song, D.; Wan, H.; Tu, X.; Li, W. A Better Understanding of Failure Process of Waterborne Coating/Metal Interface Evaluated by Electrochemical Impedance Spectroscopy. *Prog. Org. Coatings* **2020**, *142* (December 2019), 105558. https://doi.org/10.1016/j.porgcoat.2020.105558.

(17) Roggero, A.; Caussé, N.; Dantras, E.; Villareal, L.; Santos, A.; Pébère, N. Thermal Activation of Impedance Measurements on an Epoxy Coating for the Corrosion Protection: 2. Electrochemical Impedance Spectroscopy Study. *Electrochim. Acta* **2019**, *305*, 116–124. https://doi.org/10.1016/j.electacta.2019.03.007.

(18) Thomas, K. A.; Nair, S.; Rajeswari, R.; Ramesh Kumar, A. V.; Natarajan, V.; Mukundan, T.; John, R. Electrochemical Behaviour of PANi/Polyurethane Antifouling Coating in Salt Water Studied by Electrochemical Impedance Spectroscopy. *Prog. Org. Coatings* **2015**, *89*, 267–270. https://doi.org/10.1016/j.porgcoat.2015.09.007.

(19) Upadhyay, V.; Battocchi, D. Exploring the Combined Effect of DC Polarization and High Temperature Exposure on the Barrier Properties of Organic Coatings. *Prog. Org. Coatings* **2017**, *110* (April), 42–46. https://doi.org/10.1016/j.porgcoat.2017.04.026.

(20) Lin, J.; Orgon, C.; Battocchi, D.; Bierwagen, G. P. (Mg Rich Primer-Powder Topcoat) Coating System for the Corrosion Protection of Al Alloys. *Prog. Org. Coatings* **2017**, *102*, 138–143. https://doi.org/10.1016/j.porgcoat.2016.04.047.

(21) Calderon-Gutierrez, J. A.; Bedoya-Lora, F. E. Barrier Property Determination and Lifetime Prediction By Electrochemical Impedance Spectroscopy of a High Performance Organic Coating. *Dyna* **2014**, *81* (183), 97. https://doi.org/10.15446/dyna.v81n183.37609.

(22) Singh, S. K.; Tambe, S. P.; Gunasekaran, G.; Raja, V. S.; Kumar, D. Electrochemical Impedance Study of Thermally Sprayable Polyethylene Coatings. *Corros. Sci.* **2009**, *51* (3), 595–601. https://doi.org/10.1016/j.corsci.2008.11.025.

(23) Gray, L. G. S.; Appleman, B. R. EIS Electrochemical Impedance Spectroscopy - A Tool to Predict Remaining Coating Life? *J. Prot. Coatings Linings* **2003**, *20* (2), 66–74.

(24) Launer, P. J.; Arkles, B. Infrared Analysis of Orgaonsilicon Compounds. *Silicon Compd. Silanes Silicones (3rd Ed.* **2013**, 175–178.

(25) Slattery, J. C.; Peng, K. Y.; Gadalla, A. M.; Gadalla, N. Analysis of Iron Oxidation at High Temperatures. *Ind. Eng. Chem. Res.* **1995**, *34* (10), 3405–3410. https://doi.org/10.1021/ie00037a028.